2012
Number 8
ISSN 2080-5187

Civil and Environmental Engineering Reports

Prace z Inżynierii Lądowej i Środowiska

University of Zielona Góra Press, Poland

CIVIL AND ENVIRONMENTAL ENGINEERING REPORTS

Civil and Environmental Engineering Reports (CEER) is a scientific journal published semi-annually by the University of Zielona Góra.

Kindly welcome are papers that are written in English and concerned with the research problems in civil and environmental engineering.

Papers are selected for publication through the review process. The authors will receive one copy of CEER.

Templates for manuscript preparation are available on the website: *www.ceer.uz.zgora.pl*

Address of the editorial office

CEER
University of Zielona Góra
Institute of Building Engineering
ul. Z. Szafrana 1
65-516 Zielona Góra, Poland

E-mail: ceer@uz.zgora.pl
Internet: www.ceer.uz.zgora.pl

ISSN 2080-5187

Nakład – 100 egz.
Druk – Oficyna Wydawnicza Uniwersytetu Zielonogórskiego, ul. Podgórna 50, 65-246 Zielona Góra
www.ow.uz.zgora.pl

Civil and Environmental Engineering Reports

2012
Number 8

University of
Zielona Góra
Press, Poland

CONTENTS

CIVIL AND ENVIRONMENTAL ENGINEERING REPORTS

No. 8 2012

SELECTED MODELS FOR THE DESCRIPTION OF THE KINEMATICS OF CHANGES OF HEIGHT DIFFERENCES BETWEEN POINTS IN A GEODESIC NETWORK UNDER THE INFLUENCE OF MINING

Maria MRÓWCZYŃSKA*
University of Zielona Góra, Faculty of Civil and Environmental Engineering,
Institute of Building Engineering
Szafrana st 1, 65-516 Zielona Góra, Poland

The article attempts to describe the progress of deformation of the surface of the Legnica-Głogów Copper Mining Area in the years 1967-2008. The state of deformation has been described with kinematical models of the displacement of points representing the area under research. It has been analysed whether there are possibilities of using a counter-propagation algorithm for estimating displacements of selected points for which an assumption has been made that during the research they were damaged or destroyed. The numerical procedures of the estimation of parameters of displacement models were carried out by means of traditional optimisation methods and neural networks.

Keywords: neural networks, reference system, model of vertical displacements.

1. INTRODUCTION

Geodesic measurements of deformations and displacements of objects make it possible to precisely represent their geometrical condition in real spatial dimensions and to predict changes of that condition in time. Results of geodesic measurements are particularly important for research on the influence of mining on an orogenic belt and the surface of terrain. Geodesic controlling consists in determining the dynamism of the phenomenon of the displacement of controlled points which are stabilised in the research area, where there are processes caused by a change in soil-water conditions or the displacement of land masses, which happens in the case of areas and objects damaged by mining.

* Corresponding author. E-mail: m.mrowczynska@ib.uz.zgora.pl

Apart from adequate measurement equipment geodesic controlling also requires the use of correct methods of processing results of experiment data in order to correctly estimate displacements. Estimating possible displacements consists in selecting points with important displacements and points maintaining stability during measurements [8]. Defining a reference system determined at points which satisfy the criterion of stability encounters difficulties in the case of the occurrence of deformations over a large area because of the influence of unavoidable measurements errors on results of measurements of displacements of points remaining at considerable distances from one another.

2. KINEMATICAL DISPLACEMENT MODELS

The process of deformation of the surface of terrain in the Legnica – Głogów Copper Mining Are has been presented by means of functional models of kinematical networks, expressed in a general form as

$$\mathbf{H}(\mathbf{x},t)=\mathbf{L}(t) \tag{1}$$

where:

$\mathbf{H}(\mathbf{x},t)$ - component of a vector function expressing changes in height differences between the points (i,j) at the moment t,

$\mathbf{x}=[\mathbf{a}_i]\in R^n$ - vector of parameters,

$\mathbf{L}(t)=[\mathbf{l},t]\in R^m$ - observation vector,

t - real variable (time),

R^n - space of parameters,

R^m - space of measurements $(m>n)$.

Replacing a discrete set of observations of changes of height differences in a scalar form with time functions, we will analyse displacements obtained from two non-linear tendencies including time in the form [6]:

$$\mathbf{H}_1(\mathbf{x},t)=\alpha_1+\alpha_2 t+\alpha_3 t^2 \tag{2}$$

$$\mathbf{H}_2(\mathbf{x},t)=\alpha_1+\alpha_2\exp(-\alpha_3 t) \tag{3}$$

The first of the abovementioned models is a linear model, and the second, which has an exponential form, is a non-linear model. At this point it should be added that during the research topological properties of a geodesic network (defects, redundancy) together with the elimination of aberrant observations by means of a Huber function were included in each of the abovementioned models being a basis for synthetic characteristics of the displacements observed.

A basic problem in the process of determining displacements and analysing deformations is the problem of estimating a set of reference points which remain stable in terms of a random influence of measurement errors in the time interval of the research. Bearing in mind an empirical evaluation of such points, a reference system is an insignificantly flexible system, which in this paper was defined in two stages, namely [2]:

- stage I – on the basis of the minimisation of the sum of component modules of a vector of displacements obtained from equalisation with minimum restrictions on rates of freedom,
- stage II – on the basis of a criterion of an increment of the square of the norm of the vector of corrections to the observations.

Most optimisation tasks are non-linear tasks, the solution of which for research purposes requires iterative methods in almost all the cases. A numerical solution to the task of a kinematical network consists in identifying parameters of a kinematical model of geometrical components of the network which have been observed. Approximation procedures used in this case include a requirement for a minimum sum of the squares of corrections to the observations, resulting from the minimisation of the objective function

$$\sum_{i\in n}\mathbf{v}^2 = E(\mathbf{x}) = \sum_{(i,j)\in n}\left[A^{ij}\left(\alpha^i,\alpha^j,t\right) - \Delta h^{ij}(t)\right]^2 \tag{4}$$

where:

$A^{ij}\left(\alpha^i,\alpha^j,t\right) = \Delta h^j\left(\alpha^j,t\right) - \Delta h^i\left(\alpha^i,t\right)$ - component of a vector of non-linear functions which expresses a change in height differences between the points (i,j) in the time t,

n - set of points (i,j), for which the height differences Δh^{ij} were measured in the time t,

$\sum \mathbf{v}^2$ - square of the norm of the vector of corrections.

For a discretionary set of observations, the solution to the task of identifying, by means of approximation, parameters of the kinematical model (2) of changes in height differences observed is defined by a set of observation equations written in the form of vectors as

$$\mathbf{F}\left[\mathbf{x}(\boldsymbol{\alpha},t)\right] = \Delta\mathbf{h}(\boldsymbol{\alpha},t) + \mathbf{v}(\boldsymbol{\alpha},t) \tag{5}$$

Because of a linear character of the task of multinomial approximation of parameters with the use of the method of the least squares, a linearized system of equations of corrections assumes the form

$$\mathbf{A}\Delta\mathbf{x} - \Delta\mathbf{h} = \mathbf{v} \tag{6}$$

where:

$$\mathbf{A} = \frac{\partial F(\mathbf{x}_o(\boldsymbol{\alpha}, t))}{\partial \mathbf{x}_o(\boldsymbol{\alpha}, t)} \tag{7}$$

$\mathbf{x}_o$ - approximate value of the coordinates of the vector of parameters.

From the solution of the system of normal equations

$$\mathbf{A}^T\mathbf{A}\Delta\mathbf{x} = \mathbf{A}^T\Delta\mathbf{h} \tag{8}$$

we will obtain:

- estimator $\hat{\mathbf{x}}$ of the vector of parameters $\mathbf{x}$ with accuracy characteristics,
- coordinates of the vector of corrections $\mathbf{v}$,
- scaling parameter $m_0 = \sqrt{\frac{\sum \mathbf{v}^2}{m-n}}$,
- $m-n$ - number of rates of freedom of the observation.

A task of identifying parameters of kinematical models can be solved by means of neural networks, which in a number of applications play the part of a general approximator of functions of several variables. In the process of estimating parameters of the models in question an optimising neural network of a circumferential structure was used (fig. 1), which working as a one direction and recurrent network, solved the system of linear equations (6) [1, 7].

The solution of the system (6) by means of a gradient optimisation method, with the imposition of a condition of the least squares on the vector of corrections, leads to the solution of the system of differential equations [3]

$$\frac{d\mathbf{x}}{dt} = -\eta\nabla E(\mathbf{x}) = -\eta\mathbf{A}^T(\mathbf{A}\mathbf{x} - \Delta\mathbf{h}) \tag{9}$$

where:

η - learning ratio of the neural network assuming values from the range $\eta \in (0,1)$,

$\nabla E(\mathbf{x})$ - vector of the objective function (energy function) (4).

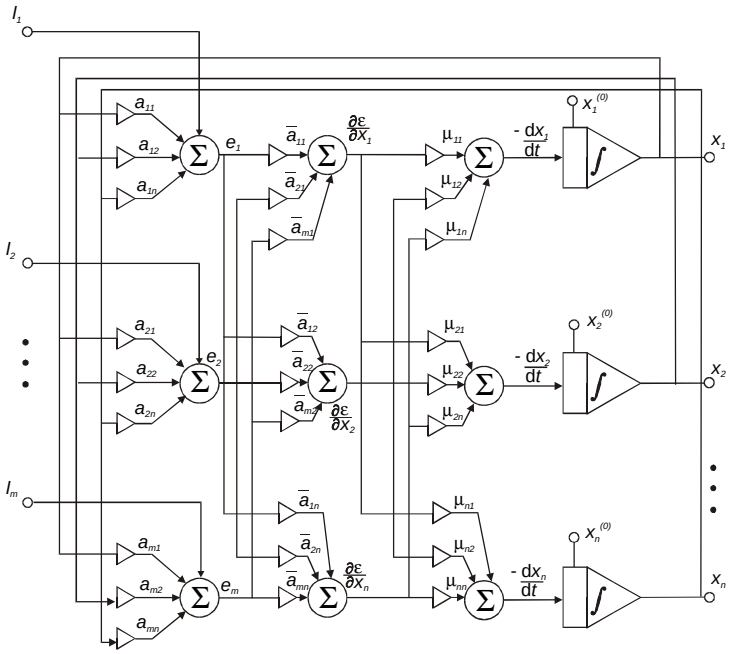

Fig. 1. Optimising a neural network of a circumferential structure [7]

The model of a kinematical network in an exponential form (3) is an implicit function which contains the transcendental function $y = e^x$. The solution of transcendental equations can be achieved by means of numerical iterative methods, because their solution can not be expressed by means of infinitesimal functions. In order to determine the estimators $\breve{\alpha}_i$ and the parameters $\alpha_i \ (i = 1,2,3)$ we will use a mean square solution, which will be obtained from the minimisation of the objective function (4). The numerical realisation of the process of estimation of parameters of the model was carried out sequentially by means of division into a linear and a non-linear model. The algorithm consists of two subsequent iterative algorithms [2]:

- estimation of the parameters $\alpha_1, \alpha_2 \in R^{2n}$ of the linear model (for $\alpha_3 = const$, i.e. $\breve{\alpha}_1, \breve{\alpha}_2 = \alpha_1, \alpha_2(\alpha_3)$),
- estimation of the parameters $\alpha_3 \in R^n$ of the non-linear model (for $\breve{\alpha}_1, \breve{\alpha}_2 = const$, i.e. $E(\alpha_1, \alpha_2(\alpha_3), \alpha_3)$).

This course of action reduces the scope of the minimisation and increases the effectiveness and reliability of the determination of a real minimum of the objective function.

In the first case for $\alpha_3 = const$, from a formal point of view, the values of parameters estimated α_1, α_2 can be obtained by means one of methods of linear algebra, and the non-linear estimator $\breve{\alpha}_3$ will be obtained e.g. by means of the procedure of the greatest fall with the use of a polynomial spline function of the second degree, used for the approximation of an objective function in a specific section and the determination of a gradient vector.

3. COUNTER-PROPAGATION NEURAL NETWORK

Among a number of types of neural networks, self-organising networks play an important role, the advantage of which is the ability to classify an input vector disturbed with noise and other disturbances. A self-organising neural network, which shows the ability to represent the function $y_i = f(x_i) + \varepsilon$ z R^n as R^m (ε - the influence of the distortion of the coordinates of the vector $\mathbf{x}$), is a counter-propagation network described by Hecht – Nielsen [4, 5] (fig. 2). Algorithms using this network have good abilities to learn a representation of the vector-vector type. The network has the ability of hetero and auto association (approximation in both directions), and as a classifier, it gives a favourable answer even if the input vector is not complete.

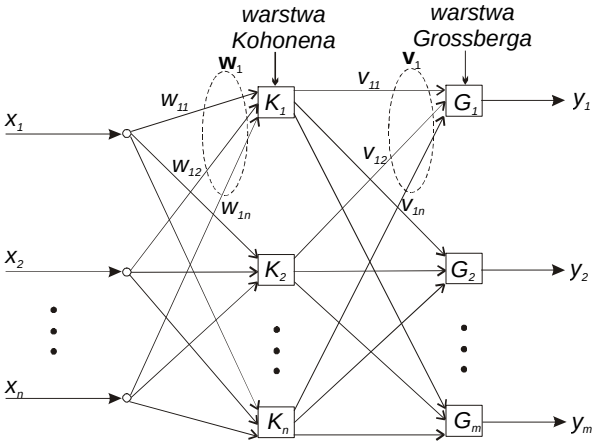

Fig. 2. Simplified structure of a Hecht – Nielsen neural network

It results from fig. 2 that the network consists of two layers: a Kohonen layer and a Grossberg layer, with a different number of neurons in particular layers. The operation of a Hecht – Nielsen network can be divided into two modes:

- the replication mode, in which we apply the vector $\mathbf{x}$ at the input, and at the output we obtain the vector $\mathbf{y}$,

- the learning mode, in which the vector $\mathbf{x}$ is accompanied by the assigned values $\mathbf{d}$ of the vector $\mathbf{y}$, and values of the vectors of weights $\mathbf{w}$ and $\mathbf{v}$, which will make it possible to represent the vector $\mathbf{x}$ as the vector $\mathbf{d}$, are searched for.

The operation of the Kohonen layer takes place in the learning mode without supervision and requires an initial normalisation of the input vector $\mathbf{x}$ according to the dependence

$$x_i = \frac{x_i}{\sqrt{\sum_{j=1}^{n} x_j^2}} \tag{10}$$

Neurons in this layer generate the weighed sum of signals

$$net_i = \sum_{j=1}^{n} w_{ij} x_j \tag{11}$$

and achieve a particular rate of activation. A neuron with the highest net_i value, which is assigned a state equal 1, wins the competition, and the state of the other vectors equals 0. In consequence of the competition won a particular neuron updates its weights according to the relation

$$w_{ij}(t+1) = w_{ij}(t) + \eta\left[x_{ij} - w_{ij}(t)\right] \tag{12}$$

where t and $t+1$ denote subsequent learning cycles, and η is a learning ratio from the range $(0,1)$.

At the second stage of the operation of the Hecht – Nielsen network, the Grossberg layer is trained in a supervised learning mode. For each pair $(x_1, y_1),\ldots,(x_m, y_m)$ only one neuron from the Kohonen layer is active, and weights coming from it are updated according to the rule

$$v_{ik}(t+1) = v_{ik}(t) + \mu\left[d_i - v_{ik}(t)\right] \tag{13}$$

where μ is a learning ratio, usually a very small one, which still decreases as learning progresses. As a result of the operation of the algorithm the values of weights v_{ik} change in the direction of the answer $y_i = v_{ik}$, corresponding to the value assigned d_i. In this case the network works as an approximator of the function $\tilde{\mathbf{y}} = f(\mathbf{x})$, which is a copy of the relation $\mathbf{y} = f(\mathbf{x})$. The mean error of the approximation for a single vector, with the assumption of an even distribution of probability of the components of the vector $\tilde{\mathbf{y}}$, is [3]

$$m = 2 - 2\sum_{i=1}^{m} v_i \tilde{y}_i \tag{14}$$

In the replication mode the network, which belongs to the class of auto-associating networks, plays the role of a function of the reciprocal association of vectors. This is so, because when we put the coordinates of the input vector x_i in the place of the values assigned d_i, we will obtain a vector $\mathbf{x}$ in the form of a vector of weights $\mathbf{v}$. If the vector $\mathbf{x}$ is an incomplete vector, then the algorithm accepts this state of affairs and generates a complete answer as a representation of a particular interpolation function. This characteristic of the algorithm was used by the authoress to determine in the network under research the values of displacements of points which were assumed to have been destroyed during the measurements.

4. NUMERICAL EXAMPLE

In order to determine displacements of measurement points located in the Legnica – Głogów Copper Mining Area results of five measurement campaigns from the years 1967-2008 were analysed. The choice of campaigns resulted from the possibility of the widest representation in terms of observations carried out. In the area under discussion of about 75000 ha 118 measurement points were located, connected with one another with 125 observations. A diagram of a measurement control network has been presented in fig.3.

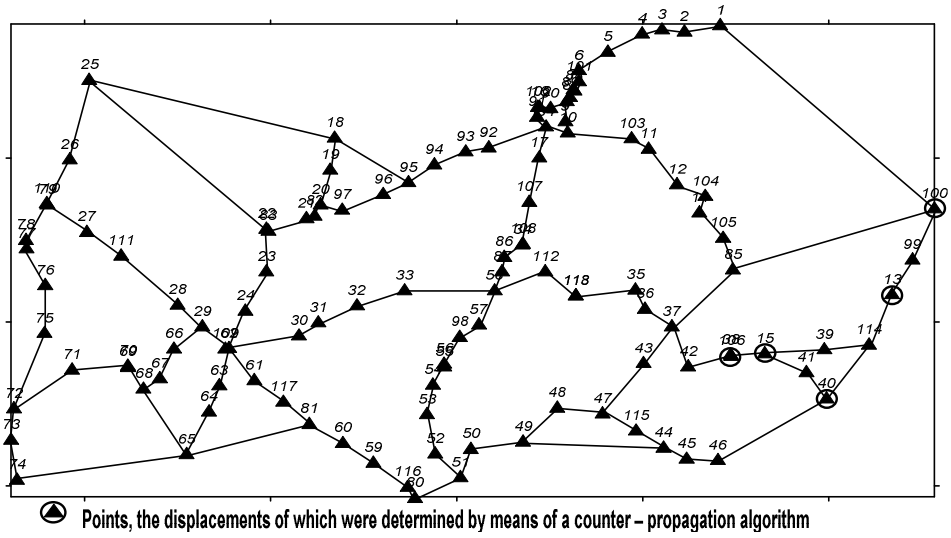

Fig. 3. Diagram of a measurement control network

As a result of the calculations in a linear and non-linear aspect values of vertical displacements of measurement points were obtained for a pre-defined reference system. The estimation of parameters of each of the two models under analysis was carried out by means of two optimisation algorithms. In order to solve the task of identification of parameters of the kinematical models (2) and (3) by means of approximation a neural network was used (fig.1), and the procedure of the least squares was used as a second method of estimating parameters of the model (2). Parameters of the model (3) were estimated by means of a hybrid method with a division into a linear and a non-linear model with the use of the method of the greatest fall.

Characteristics of the accuracy of the abovementioned methods of representation of functional models in the form of a mean approximation error are as follows:

1. linear model (2):
   - neural network $m_0 = 1{,}4$ mm
   - method of the least squares $m_0 = 1{,}4$ mm
2. non-linear model (3):
   - neural network $m_0 = 2{,}0$ mm
   - hybrid method $m_0 = 1{,}9$ mm

In time intervals of the research the displacement values determined are between +84,5 mm to -3851,3 mm, and the maximum speed of displacements is on the level of 88 mm/year. The displacements with the line of steady fall and speed including the range of maximum values have been illustrated respectively in fig.4 and 5.

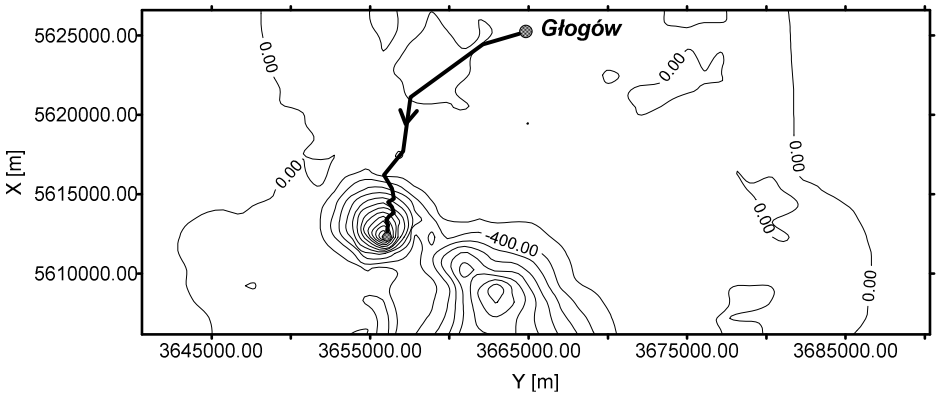

Fig. 4. Kinematical displacement model obtained for the period of time 1967 – 2008 with the line of the greatest fall

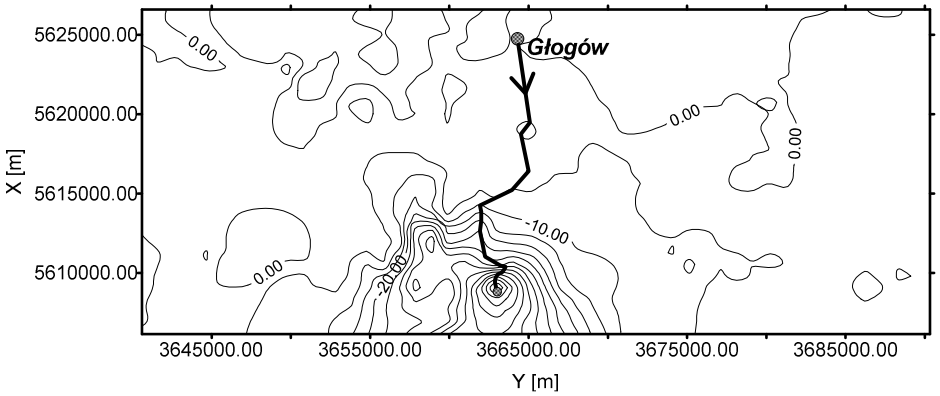

Fig. 5. Speed of displacements of controlled points in mm/year with the line of the greatest displacement speeds

In the case of an incomplete data set (damage or destruction of measurement points), a Hecht – Nielsen neural network based on counter-propagation can be used to generate a relatively correct vector of displacements. A result of the use of a counter-propagation algorithm has been presented for one of the measurement sequences of 12 points, with the assumption that as a result of damage or destruction 5 points were unavailable for measurement in the years 2004 – 2008. The mean error of the approximation calculated from the formula (14), for the measurement period 1967 – 2004 was 0,37, and for the measurement period 1967 – 2008 - 0,74. Particular values of displacements obtained from the measurement for the model (2) and reproduced by means of the counter-propagation algorithm have been presented in table 1, and represented graphically in fig.6 and fig. 7.

Table 1. Values of displacements obtained by means of the counter-propagation algorithm

Point number	Displacements obtained from measurements in particular measurement periods [mm]				Displacements reproduced [mm]	
	1967-1998	1967-2000	1967-2004	1967-2008	1967-2004	1967-2008
13	-0,87	-1,45	-1,76	-2,34	-1,61	-2,28
15	-10,14	-12,08	-14,24	-16,08	-14,04	-16,22
40	-7,24	-8,94	-12,08	-15,26	-11,48	-13,57
86	-9,78	-11,84	-14,23	-16,17	-14,29	-16,08
100	-0,95	-1,15	-1,12	-1,10	-1,34	-1,46

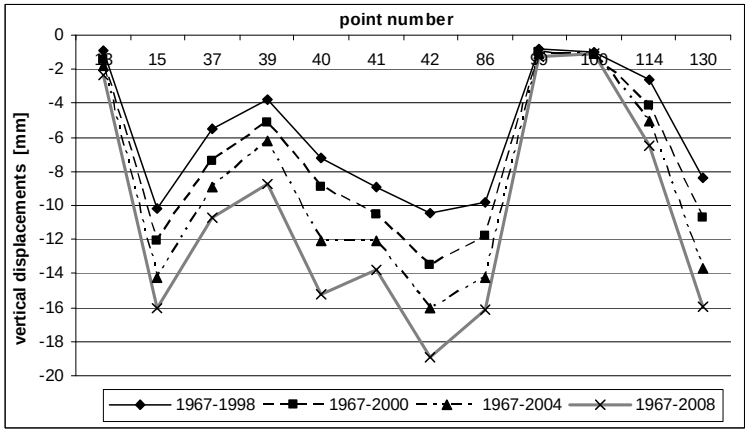

Fig. 6. Vertical displacements of measurement [mm]

While comparing the values of displacements obtained from the measurement with the displacements reproduced by means of the Hecht – Nielsen network, it is possible to notice that the smallest differences can be found in the case of points 13 and 86, for which values of the speed of displacements within the whole measurement period are small. The greatest difference - 1,69 mm occurs at point No. 40. This situation is most likely caused by a considerable speed of settlement of this point in the years 2004 and 2008, in comparison to the speed of displacements obtained in the previous years (cf. fig. 6).

The values of vertical displacements reproduced for selected controlled points by means of the method of counter – propagation have been presented graphically in fig. 7.

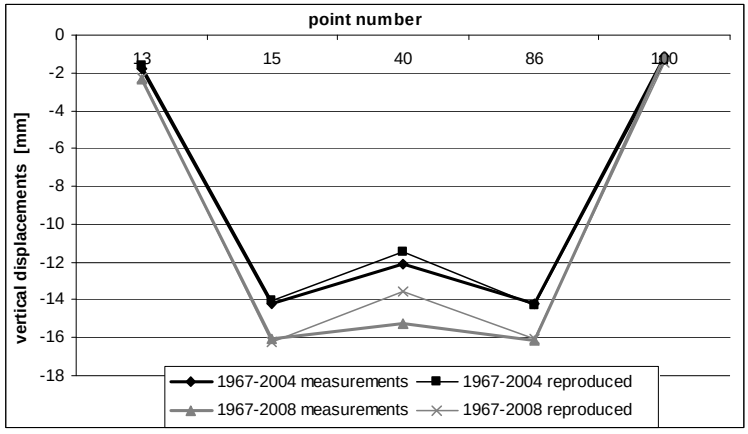

Fig. 7. Values of displacements of points No. 13, 15, 40, 86, 100 for the periods of time 1967 – 2004 and 1967 – 2008 reproduced by means of counter propagation

Prediction of values of displacements by one step for the measurement period 1967 – 2010 has been presented graphically in fig.8. It should be noticed that values of displacements determined on the basis of an exponential curve increased at the most by 92 mm for point *P* marked in fig. 8.

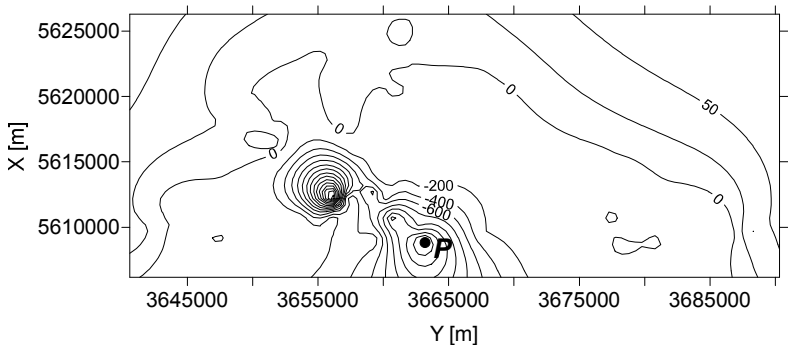

Fig 8. Prediction of displacements for the area under discussion in the year 2010

5. CONCLUSIONS

Values of vertical displacements of measurement points located in an area influenced by mining presented in the paper make it possible to say that displacements obtained by means of kinematical models, the parameters of which were estimated by means of a neural network do not differ in terms of quality from displacements obtained by means of traditional methods of optimisation. By means of a counter – propagation neural network it is possible to reproduce, with a particular level of approximation, displacements of points which were damaged or destroyed during the measurements. However, it is necessary to notice that the speed of changes occurring influences the accuracy of displacements reproduced. If the speed is steady during the whole time of measurements, then the accuracy of the reproduction of displacements is much higher than in the case of rapid accelerations of the settlement process. Research into vertical displacements of the surface of terrain caused by mining, together with exogenous factors, justifies the adoption of non-linear models of movement, because the cause and effect relationships between reactions of variables occurring in nature are non linear relationships.

REFERENCES

1. Gibowski S.: *Kinematyka wysokościowej sieci pomiarowo kontrolnej w aspekcie zastosowania algorytmów klasycznych i sieci neuronowych*, Rozprawa doktorska, Wrocław 2008.

2. Gil J.: *Badanie nieliniowego geodezyjnego modelu kinematycznego przemieszczeń*, seria: monografie nr 76, Wydawnictwo WSI w Zielonej Górze, Zielona Góra 1995.
3. Gil J.: *Przykłady zastosowań sieci neuronowych w geodezji*, Oficyna Wydawnicza Uniwersytetu Zielonogórskiego, Zielona Góra 2006.
4. Hecht – Nielsen R.: *Counterpropagation networks*, Network Applied Optocs, vol.26 1987.
5. Hecht – Nielsen R.: *Applications of counterpropagation networks*, Neural Networks, vol. 1, 1988.
6. Kadaj R.: *Modele, metody i algorytmy obliczeniowe sieci kinematycznych w geodezyjnych pomiarach przemieszczeń i odkształceń obiektów*, Wydawnictwo AR Kraków 1998.
7. Osowski S.: *Sieci neuronowe*, Oficyna Wydawnicza Politechniki Warszawskiej., Warszawa 1996.
8. Prószyński W., Kwaśniak B.: *Podstawy geodezyjnego wyznaczania przemieszczeń*, Oficyna Wydawnicza Politechniki Warszawskiej, 2006.

WYBRANE MODELE OPISU KINEMATYKI SIECI GEODEZYJNEJ WYSOKOŚCIOWEJ POD WPŁYWEM EKSPLOATACJI GÓRNICZEJ

S t r e s z c z e n i e

W treści artykułu podjęto próbę opisu przebiegu deformacji powierzchni terenu obszaru Legnicko – Głogowskiego Okręgu Miedziowego w latach 1967 – 2008. Stan deformacji został opisany modelami kinematycznymi przemieszczeń punktów reprezentujących badany obszar. Przeprowadzono rozważania dotyczące możliwości wykorzystania algorytmu kontrpropagacji do oszacowania przemieszczeń wybranych punktów, dla których przyjęto założenie, że w trakcie prowadzonych badań punkty zostały uszkodzone bądź zniszczone. Procedury numeryczne estymacji parametrów modeli przemieszczeń realizowano za pomocą tradycyjnych metod optymalizacji i sieci neuronowych.

CIVIL AND ENVIRONMENTAL ENGINEERING REPORTS

No. 8 2012

TRANSFORMATIONS OF ORGANIC COMPOUNDS IN THE OPEN INTERCEPTING SEWER

Sylwia MYSZOGRAJ[1*], Zofia SADECKA[1],
Monika SUCHOWSKA-KISIELEWICZ[1],
Ewelina PŁUCIENNIK-KOROPCZUK[1], Omar QTEISHAT[2]
[1]University of Zielona Góra, Faculty of Civil and Environmental Engineering,
Institute of Environmental Engineering
Szafrana st 15, 65-516 Zielona Góra, Poland
[2]Al-Balqua' Applied University, Zarka University College, Jordania

The paper presents results of studies concerning the designation of COD fraction in the raw wastewater. The test object was open intercepting sewer of Zielona Góra. Methodology for determining the COD fraction was based on the guidelines ATV- A 131. The real concentration of fractions in raw wastewater and the percentage of each fraction in total COD are different from data reported in the literature. The processes occurring in an open interceptor are also influenced by external factors. The most important of them are the ambient temperature and the extent of solar exposure. The changing temperature influences solubility of oxygen and activity of micro-organisms. Open space and cascade arrangement of the interceptor decrease the probability of oxygen-free environment. In this case, the dominating significance in the decomposition of organic compounds is to be ascribed to oxygen processes.

Keywords: biochemical process, dissolved oxygen, COD fraction, open intercepting sewer, cascade

1. INTRODUCTION

The main function of a sewerage system is reception and channelling of sewage to a wastewater treatment plant (WWTP), or a receiver. Currently, more and more frequently, a sewerage systems is analysed in the context of biochemical processes which take place therein. A sewer which carries sewage to WWTP can be treated as a flow sewage receiver, and it can be assumed that this is where transformations the basis of which are self-purification processes, occurring in

* Corresponding author. E-mail: s.myszograj@iis.uz.zgora.pl

rivers, take place. Changes in the composition of sewerage in sewage system can significantly influence operation of treatment plants and receivers of treated sewage.

Hydrolysis of organic compounds, increase in biomass of microorganisms, alterations in fractions of organic substance, as well as sedimentation of suspended matters are processes which take place during transport of sewage through a sewage system, and which directly influence quality of the sewage incoming to the treatment plant. These processes occur in water environment, in deposits, bacterial jelly which form on the inside walls of a sewer, and their intensity depends, among other factors, on the type and length of the sewage system. The processes occurring in sewers are presented in Fig. 1 [1,4].

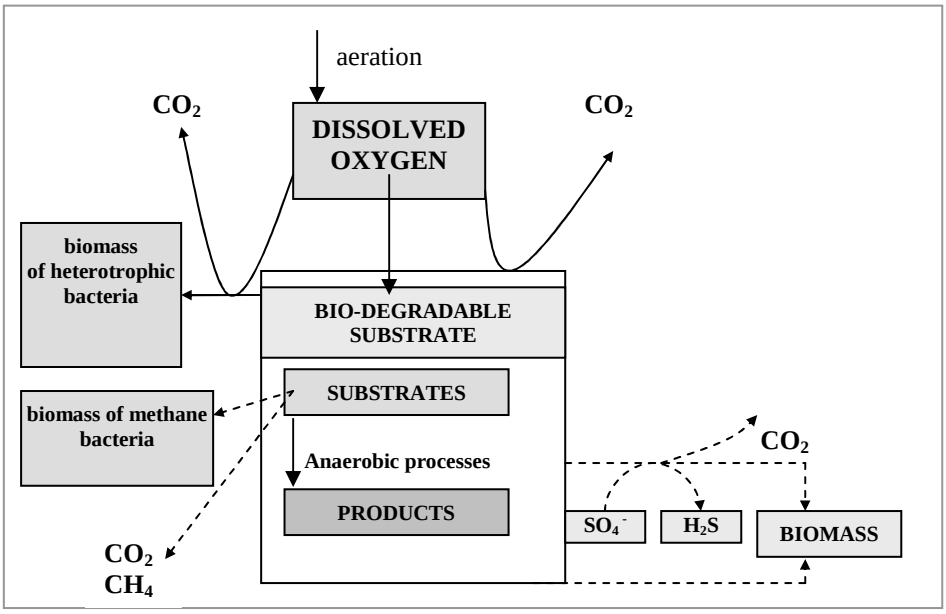

Fig. 1. Microbiological transformations of organic compounds in sewage system, in aerobic/anaerobic processes

Due to high concentration of pollutions, biochemical changes proceed slowly, and the result of treatment of sewage during its transport will be determined by intensifying interference of human. Decomposition of organic compounds occurs the most intensively in oxygen environment, between the layer of bottoms and the flowing sewage. These processes cause significant decrease in sewage contamination. Both at the cellular level, and at the ecosystem level, the processes of transforming organic substrates require hydrolysis of insoluble organic polymers into soluble forms, available for

microorganisms. Part of the pollutants undergo direct, biochemical oxidation into carbon dioxide and water, while the remaining fraction is assimilated in the form of increase in the living mass of the microorganisms [2,3].

Sewage transported via the sewage system contain various groups of microorganisms, the development of which depends on specific environmental conditions. Living organisms which dwell in the bottoms often manifest high metabolic activity, participating in the process of biodegradation of various organic contaminations contained not only in the deposits, but also in the sewage which flows through the system.

Chemical and biological processes in the intercepting sewers can significantly influence the composition of the sewage, particularly during rainless stretches. In an anaerobic processes, next to an increase in concentration of sulphur compounds, transformations of organic matter into easily-biodegradable substrates, which are a notable base of effective denitrification and biological dephosphatation, gain crucial importance. Whereas in oxygen processes, concentration of biodegradable fraction of organic biomass decreases, and heterotrophic biomass which can be effectively removed in the mechanical section of a treatment plant, increases [4].

The application of modern technologies requires thorough identification of the composition of substrates present in sewage, as compared to data obtained with conventional pollution indicators ($COD\text{-}_{Cr}$, BOD_5) [5,6]. One of the most significant achievements in sewage technology is COD fractioning, which makes it possible to isolate fractions depending on the size of molecules and their responsiveness to biochemical decomposition [7,8]. Determination of COD fractions furnishes a detailed characteristic of sewage composition, but primarily makes it possible to determine the amount of organic contaminants, both easily and poorly degradable [9].

Changes in the physical-chemical characteristics of sewage in a sewage system are presented on the basis of studying an open sewer which channels sewage from Zielona Gora (Poland) to a wastewater treatment plant in Lezyca.

2. MATERIAL AND METHODS

2.1. Open sewage channel to WWTP in Lezyca

Zielona Gora (Poland) has 118 221 inhabitants. Branches of the industrial sector typical for the city are: textile industry (wool, ornamental fabric, sheet flooring), production of means of transport (freight cars), food industry (distilling, winemaking, dairy, meat, brewery), precision industry, furniture industry.

The central sewage treatment plant for Zielona Gora is situated about 7km north of the city, and west of the Lezyca village.

The treatment plant of flow capacity $Q = 51.225\ m^3/d$ has been designed for mechanical-biological sewage treatment, with biological dephosphatation,

denitrification and nitrification, as well as chemical precipitation of the remaining phosphorus.

The sewage are channelled to the wastewater treatment plant via an open sewer. The course of the open sewer runs outside the city borders (Fig. 2).

Fig. 2. Plan of Zielona Gora, with marking of the open sewer which carries raw sewage to WWTP

The length of the open sewer is 4850 m. Due to significant altitude difference between the start and the end of the sewer, it has been partitioned with cascades, which form six sections: first - 700 m long, second - 258 m, third - 742 m, fourth - 500 m, fifth - 1000 m, sixth - 1650 m. The stilling basius constructions form five storage reservoirs, with total capacity of 84 000 m^3.

The average sewage flow rate for the entire sewer is 0,9 m/s (for rainless periods), whereas the average time of sewage flow through the open channel is 1,5h. During intensive rainfall, the rate increase to about 2,0 m/s.

2.2. Analytical methods

Analysis of physical-chemical composition of the sewage collected from the open sewer which channels sewage from Zielona Gora to treatment plant in Lezyca was carried out five times.

Sewage sampling was planned in a period preceded with several rainless days. The ambient temperature changed as follows:
Series 1 – ambient temperature 17 ^{o}C, sunny
Series 2 – ambient temperature 20 ^{o}C, heavy clouds
Series 3 – ambient temperature 10 ^{o}C, heavy clouds
Series 4 – ambient temperature 12 ^{o}C, partly cloudy
Series 5 – ambient temperature 16 ^{o}C, partly cloudy

In each series of the study, 7 samples of sewage were taken from the open sewer: first sample at the beginning of the open sewer, samples 2, 3, 4, 5, 6 directly after subsequent cascades, whereas the final sample 7 was taken at the end of the open sewer (Fig. 3).

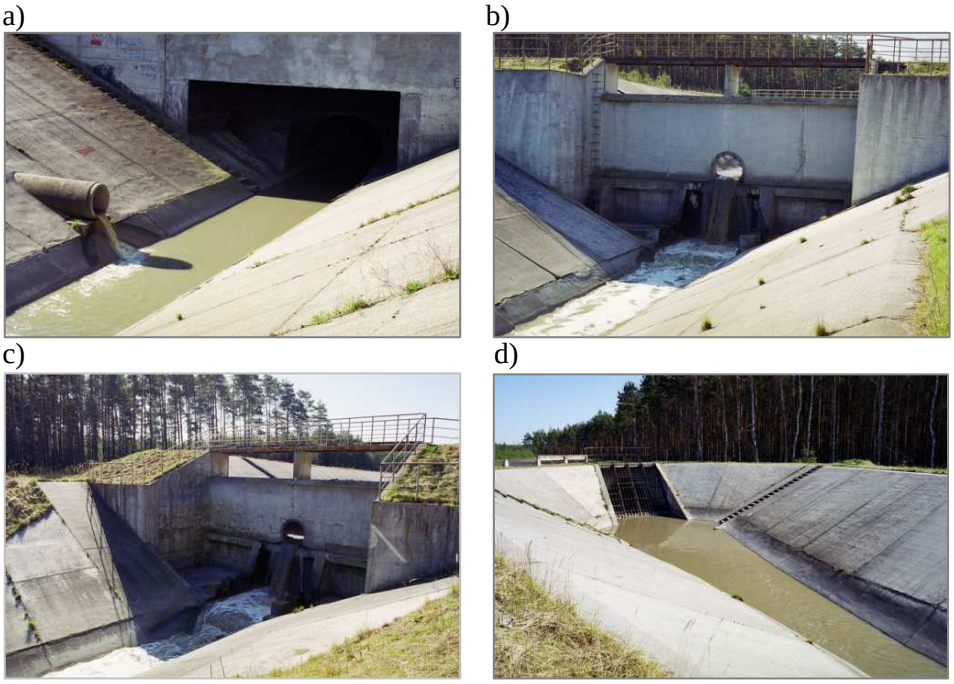

Fig. 3. View of the open sewer which channels sewage to WWTP in Lezyca
a) beginning of the open sewer - measuring point 1, b) measuring point 2,
c) measuring point 3, d) end of the open sewer - measuring point 7

The following parameters were marked in the sewage samples: concentration of dissolved oxygen (DO), Chemical Oxygen Demand (COD), Biochemical Oxygen Demand (BOD_5). The analyses were made of the method applicable in Poland.

In every series, collection of sewage from the first measuring point was made at 09.00. The next samples were taken after a time which takes into account the speed of sewage in the channel. Concentration of dissolved oxygen, pH and sewage temperature were measured directly in the intercepting sewer.

On the basis of the designated values BOD_5 and COD, organic compounds were divided into suspension and dissolved fractions, as well as into easily and slowly biologically degradable. COD of the sewage, with division into fractions, can be calculated in a simplified manner in accordance with the following dependence [6]:

$$COD = S_S + S_I + X_S + X_I \quad (1)$$

S_S - COD of dissolved organically compounds, easily biodegradable,
S_S - COD of dissolved organically compounds, non-biodegradable,
X_S - COD of organic suspensions, slowly-degradable,
X_I - COD of organic suspensions, non-degradable.

The methodology of determining the COD fraction was developed on the basis of guidelines ATV-131 [Commentary on ATV - A131, 2000].
It should be stressed that assessment of the values of contamination indexes and COD fraction for samples of sewage taken directly from the intercepting sewer is a difficult and subjective assessment, depending on numerous external factors related to sampling, daytime, day of the week (unevenness of water consumption), and for complete orientation and comparison, it requires a lot of results from each point.

3. RESULTS

On the basis of the performed measurements of dissolved oxygen concentration (Fig. 4), directly past each cascade, it has been found that it gradually increases between the start of the open interceptor and the 4the (5^{th}) cascade.

In sewage transported through the sewer between the 5^{th} cascade to the 7^{th} measuring point (longest distances between cascades), concentration of DO is lower.

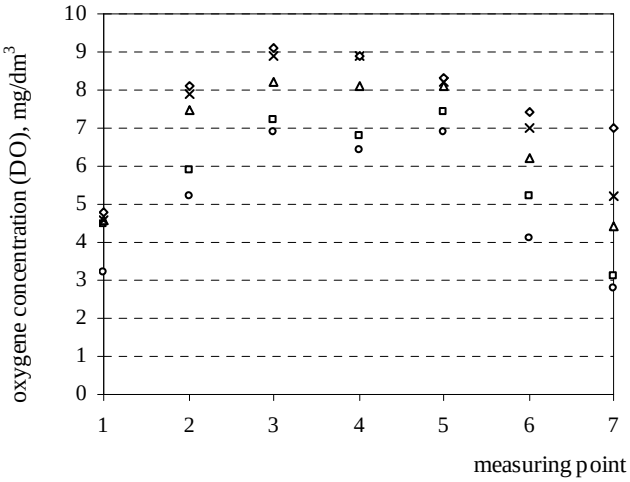

Fig. 4. Changes of DO in the sewage in 5 series

Changes of COD and BOD_5 in the sewage in open intercepting sewer are presented graphically in Fig. 5.

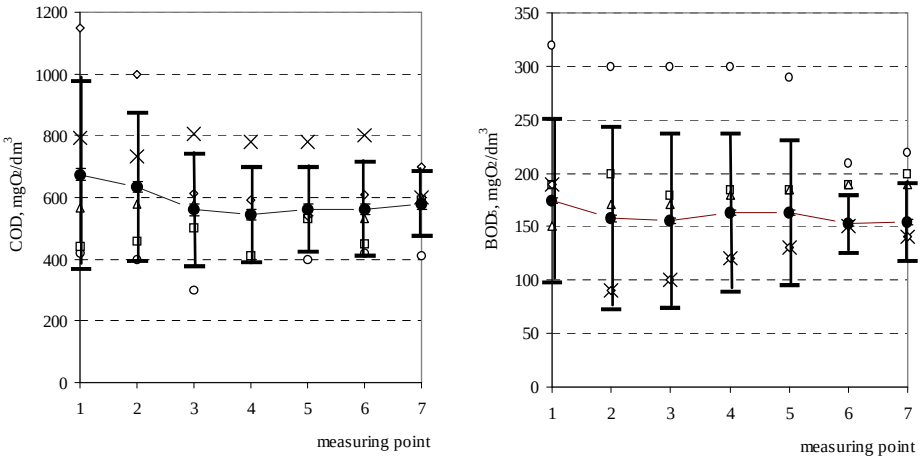

Fig. 5. Changes in COD and BOD_5 in the sewage at measuring points (5 series) and standard deviation of average values

The average (specified on the basis of 5 measurements) value of total COD in the sewage at sections of the open intercepting sewer (measured at points 1 to 7) changed from 674 to 544 mgO_2/dm^3 between point 1 and 6, to reach the value of 577 mgO_2/dm^3 at the end of the interceptor. The amount of

organic compounds in the sewage expressed as average BOD_5 ranged between 181 and 150 mgO_2/dm^3.

Average values of COD fraction in the sewage at subsequent measuring points is shown in Table 1. Share of the inert fraction COD ($X_I + S_I$) (Fig. 6.) changed from 13 to 20%, and biodegradable substance ($X_S + S_S$) in the sewage was between 80 and 87%.

The amount of dissolved biodegradable substance ranged from 30 to 35%. Share of dissolved fraction ($S_S + S_I$) in $COD_{tot.}$ varied from 31 to 39%, whereas the share of the suspension fraction ($X_S + X_I$) – from 64 to 71%.

Table 1. Average values of COD fraction in the sewage at subsequent measuring points

COD fraction, mgO_2/dm^3	measuring point						
	1	2	3	4	5	6	7
S_s	235	185	191	191	194	160	179
S_i	2	9	1	5	4	3	9
X_i	67	90	79	94	93	85	91
X_s	370	351	291	254	256	315	298
Sum	674	635	562	544	547	563	577

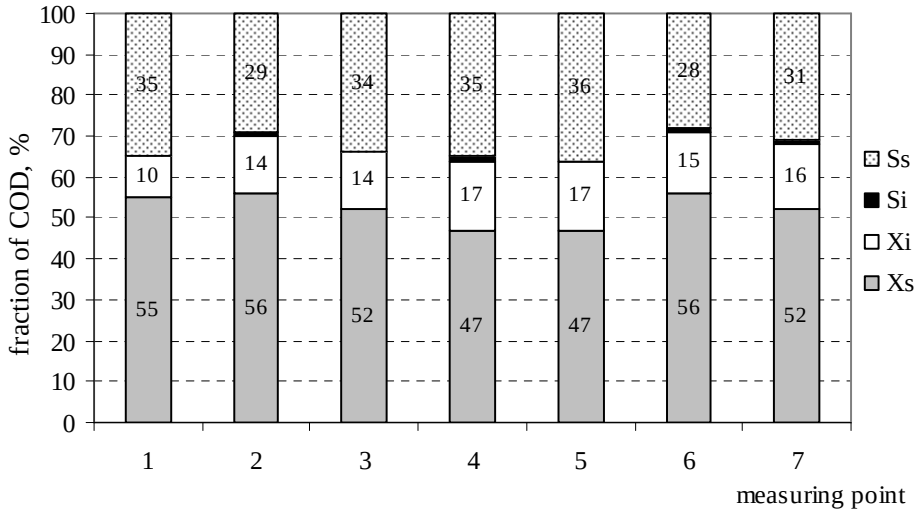

Fig. 6. Average values of COD fraction in the sewage at subsequent measuring points [divided into fractions in %]

Analysis of the obtained values of individual COD fractions, depending on the point of collecting the sample, demonstrated, that comparable results were achieved for all five series. It was also found that regardless of the COD and

BOD_5 values in raw sewage channelled via open sewer, distribution of individual COD fractions in all the series was very similar.

The presented research results demonstrate that during transportation of sewage through an open sewer, changes in the composition thereof take place. Significant differences were found for COD and BOD_5 of the sewage.
During the research period, the highest extent of decrease in the sewage COD value within the channel was 35%, and for BOD_5 – 33%.

4. CONCLUSION

The processes occurring in an open interceptor are influenced by internal and external factors. The most important are the ambient temperature and the extent of solar exposure. The changing temperature influences solubility of oxygen and activity of micro-organisms. Open space and cascade arrangement of the interceptor decrease the probability of oxygen-free environment. In this case, the dominating significance in the decomposition of organic compounds is to be ascribed to oxygen processes.

The sewage treatment processes begin already in the sewer and they can positively influence operation of the treatment plant. It should be remembered that the conditions of sewage flow are changeable, and modelling of changes as well as effective use of an open interceptor as a biological reactor require further, detailed research.

REFERENCES

1. Ashley R., Hvitved-Jacobsen T., Krajewski J.L.B.: *Quo vadis sewer process modelling?* Wat.Sci.Tech., **39**, 9 (1999) 9-22.
2. Dąbrowski W.: *Oddziaływanie sieci kanalizacyjnych na środowisko*. Kraków, Politechnika Krakowska im. T. Kościuszki, 2004.
3. Henze M., Gujer W., Mino T., Matsuo T., Wentzel M.C., Maras R.: *Wastewater and biomass characterization for the activated sludge model no.2: biological phosphorus removal*. Wat.Sci.Tech., **31**, 2 (1995) 13-23.
4. Hvitved-Jacobsen T., Vollertsen J., Nielsen P.H.: *A process and model koncept for microbial wastewater transformations in gravity sewers.* Wat.Sci.Tech., **37**, 1 (1998) 233-241.
5. Myszograj S.: *Bilans ChZT w biologicznym oczyszczaniu ścieków osadem czynnym - cz. I. skala laboratoryjna.* w: Zeszyty Naukowe Uniwersytetu Zielonogórskiego, Inżynieria Środowiska, **140**, 20 (2010) 102-111.

6. Orhon D., Ates E., Sözen S., Cokgör E.U.: *Characterization and COD fractionation of domestic wastewater*,. Environmental Pollution, **95**, 2 (1997) 191-204.
7. Qteishat O., Myszograj S., Suchowska-Kisielewicz M.: *Changes of wastewater characteristic during transport in sewers*. WSEAS Transactions on Environment and Development, **7**, 11 (2011) 349-358.
8. Sadecka Z., Płuciennik-Koropczuk E., Sieciechowicz A.: *Charakterystyka ścieków surowych na podstawie frakcji ChZT*. Engineering and Protection of Environment, **14**, 2 (2011) 145-156.
9. Vollertsen J., Hvitved-Jacobsen T., McGregor I., Ashley R.: *Aerobic microbial transformations of pipe and stil trap sediments from combined sewers.* Wat.Sci. Tech., **38**, 10 (1998) 249-256.

PRZEMIANY ZWIĄZKÓW ORGANICZNYCH W OTWARTYM KANALE ŚCIEKOWYM

S t r e s z c z e n i e

Głównym zadaniem sieci kanalizacyjnych jest odbiór i odprowadzenie ścieków do oczyszczalni lub odbiornika. Obecnie coraz częściej sieć kanalizacyjna jest analizowana w aspekcie zachodzących w niej procesów biochemicznych. Kanał doprowadzający ścieki do oczyszczalni można potraktować jak przepływowy odbiornik ścieków i przyjąć, że zachodzą w nim przemiany, których podstawą są procesy samooczyszczania zachodzące w rzekach. Zmiany w składzie ścieków w kanalizacji mogą w istotny sposób wpływać na pracę oczyszczalni i odbiornik ścieków oczyszczonych.

W artykule przedstawiono wyniki badań zmian charakterystyki ścieków surowych dopływających do oczyszczalni ścieków kanałem otwartym. Ustalono, że na procesy zachodzące w kolektorze otwartym znaczący wpływ mają czynniki zewnętrzne. Najważniejszym z nich jest temperatura otoczenia i stopień nasłonecznienia. Temperatura ścieków wpływa na rozpuszczalność tlenu w ściekach i aktywność mikroorganizmów. System kaskadowego przepływu ścieków w kolektorze zmniejsza prawdopodobieństwo wystąpienia warunków beztlenowych.

CIVIL AND ENVIRONMENTAL ENGINEERING REPORTS

No. 8 2012

PEAKING FACTORS OF DRY WEATHER FLOWS IN GŁOGÓW COMBINED SEWAGE SYSTEM

Ireneusz NOWOGOŃSKI*, Ewa OGIOŁDA
University of Zielona Góra, Faculty of Civil and Environmental Engineering,
Institute of Environmental Engineering
Szafrana st 15, 65-516 Zielona Góra, Poland

This paper presents the results of dry weather flowrate studies in inflow and outflow channels of overflow structure PB-1. The facility is located in P.Skargi Street in Głogów. Based on the results the average daily peaking factor of dry weather sewage outflow was estimated. Low efficiency of the algorithm allows the estimation of the flow when depth of the channel is less then 20 cm and when it is not possible to perform measurements with the ultrasound probe. Pointed to inadequate reconstruction of cross-sectional shape of the channel during device configuration as the cause of getting inconsistent results. The results of corrective calculations based on Manning's formula and typical cross-sections of channels were presented. Obtained results confirm the possibility of significant differences obtained when the channel parameters are configured incorrectly. Confirmed the low quality of the built-in algorithm supporting measurements at low depths, mistakenly called by the device manufacturer "Manning's formula method".

Keywords: combined sewage system, dry weather flowrate, peaking factor

1. INTRODUCTION

In designing of sewer systems, good estimation of design maximum flowrates are very important. Sewer system needs to have capacity large enough to accommodate increased domestic flows associated with increases of population and system expansion (Moulton 1999). Good estimation of minimum flowrates are valuable when designing combined sewer system. If the flowrate is too small, solid deposits can become substantial and adequate self-cleaning isn't achieved. Analising of existed systems is connected with choosing adequate measurement equipment. The use of profiling flowmeters to measure flowrate in

* Corresponding author. E-mail: i.nowogonski@iis.uz.zgora.pl

the channels seems to be a very good solution. Advanced algorithms for auto-calibration, measurement using more than one ultrasonic probe, suggests the possibility to obtain reliable results. In practice, it turns out that despite the higher cost repeatedly obtained results are far from ideal. The least reliable results are obtained when the small depth is observed. In theory, the method of calculating the flow rate using the Manning's formula is used here. Practically, algorithms that generate the flow curves, based on measurements of large fillings are used. As a result, incorrect results are obtained and their use is not possible.

2. RESULTS

The study was conducted in city Głogów with population of about 67 thousands people located in Dolnośląskie Province 60 km away from Zielona Góra. The combined sewer system serves an area of 3511 ha. Analyzed sewer system in Głogów is equipped with three combined sewer overflows with single side weir and one flow divider connected with storage facility.

Rainfall was measured by six tipping-bucket rain gauges (Fig. 1). Measurements were taken in all seasons of the year.

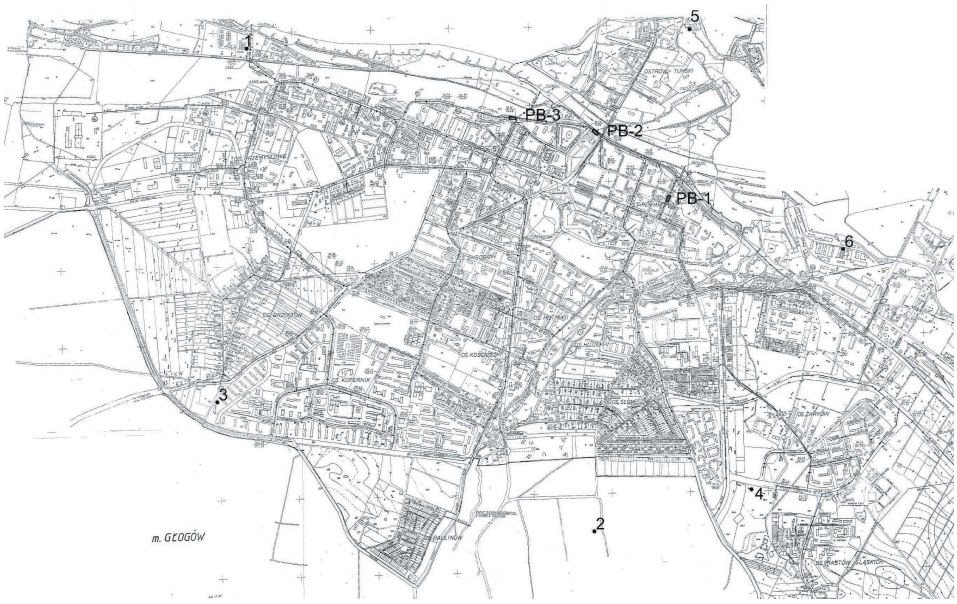

Fig. 1. Locations of rain gauges and overflow structures in the city

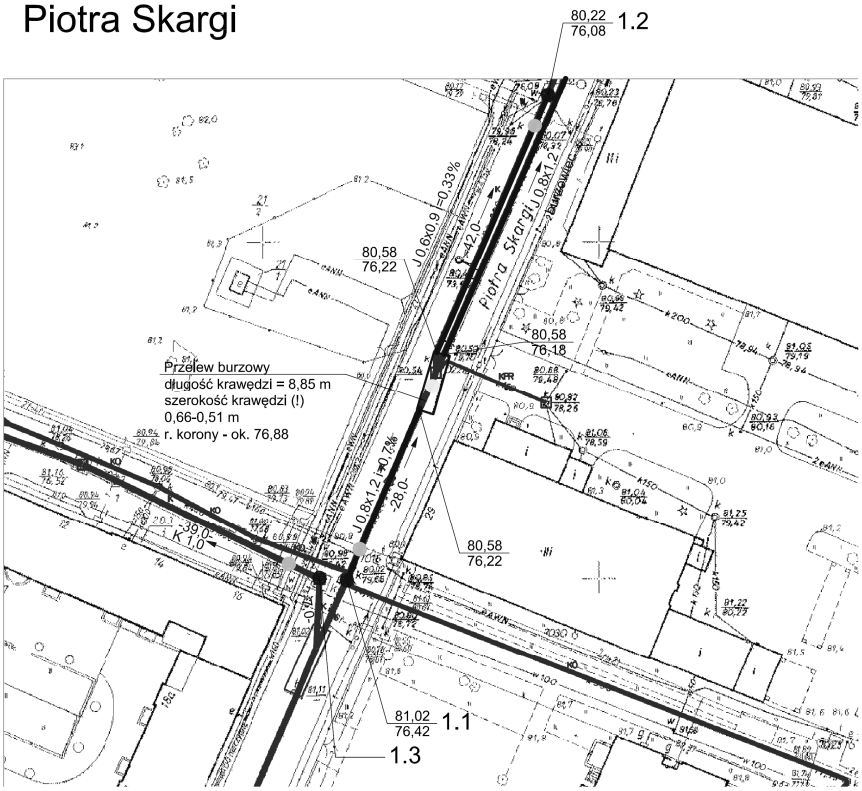

Fig. 2. Locations of flowmeters near overflow structure PB-1

Tab 1. Specification of dry weather minimum and maximum flow rates [lps]

Month	Skargi 1.1		Skargi 1.2	
	min	max	min	max
10.2011	5	64	12	56
11.2011	5	29	12	56
12.2011	6	52	12	47
01.2012	13	54	12	46
02.2012	14	60	12	51
03.2012	-	-	12	52
04.2012	13	55	12	45
05.2012	-	-	10	55
06.2012	11	51	12	44
07.2012	8	64	5	51

Tab 2. Specification of dry weather minimum and maximum depth [mm]

Month	Skargi 1.1		Skargi 1.2	
	min	max	min	max
10.2011	77	176	134	262
11.2011	77	160	132	252
12.2011	80	145	132	242
01.2012	86	151	135	224
02.2012	83	153	139	238
03.2012	-	-	143	244
04.2012	85	150	135	229
05.2012	-	-	132	233
06.2012	82	148	135	231
07.2012	98	164	137	248

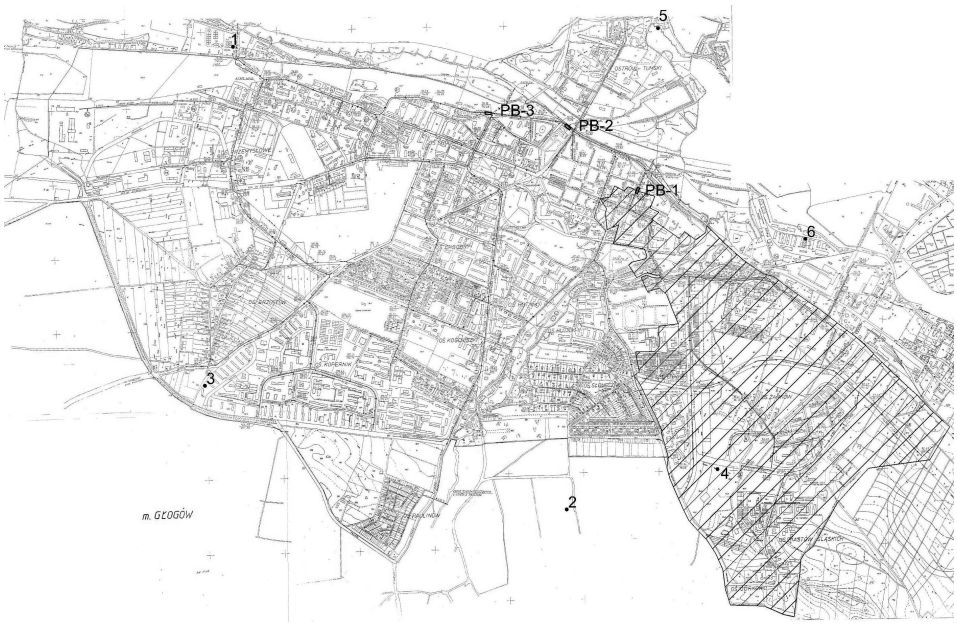

Fig. 3. Subcatchment connected with overflow structure PB-1

Flow rates were measured by ISCO ultrasonic profiling flow meters located at sewer manholes upstream and downstream of the CSO chambers. Special attention was taken to avoid improper installation of the ultrasonic probes (e.g., in sections with backwater effects or places with large amounts of sediments). All instruments were equipped with data loggers, which were fully synchronised and set for 5 min recording intervals. Locations of analysed flowmeters were shown on Figure 2.

Tab 3. Dry weather peaking factors estimation

Date	Flow rates – Skargi 1.1			Flow rates – Skargi 1.2		
	maximum	average	peaking factor	maximum	average	peaking factor
14.10.2011	56,0	40,2	1,39	43,0	24,1	1,79
16.10.2011	49,0	34,4	1,42	48,0	24,7	1,94
29.10.2011	22,0	15,9	1,39	39,0	25,2	1,54
31.10.2011	22,0	15,0	1,47	36,0	24,8	1,45
05.11.2011	22,0	16,2	1,36	40,0	14,0	1,51
15.11.2011	22,0	14,5	1,52	36,0	22,6	1,60
27.11.2011	21,0	14,5	1,45	39,0	24,3	1,61
29.11.2011	25,0	14,2	1,76	42,0	23,2	1,81
26.12.2011	52,0	34,6	1,50	43,0	24,0	1,79
31.01.2012	54,0	35,8	1,51	42,0	25,1	1,67
04.02.2012	50,0	35,6	1,41	51,0	26,4	1,93
07.02.2012	51,0	34,3	1,49	37,0	23,4	1,58
20.02.2012	-	-	-	41,0	25,5	1,61
02.03.2012	-	-	-	35,0	23,4	1,50
03.03.2012	-	-	-	52,0	25,8	2,02
04.03.2012	-	-	-	45,0	23,2	1,94
05.03.2012	-	-	-	35,0	22,0	1,59
07.03.2012	-	-	-	43,0	22,4	1,92
15.03.2012	-	-	-	43,0	24,3	1,77
20.03.2012	-	-	-	43,0	24,3	1,77
01.04.2012	47,0	32,4	1,45	37,0	22,4	1,65
11.04.2012	55,0	36,7	1,50	45,0	22,0	1,50
02.06.2012	47,0	32,4	1,45	44,0	24,5	1,80
24.07.2012	53,0	38,5	1,38	41,0	23,2	1,77
25.07.2012	54,0	37,6	1,43	44,0	24,8	1,90
26.07.2012	52,0	36,6	1,42	40,0	20,5	1,95
27.07.2012	56,0	37,5	1,49	51,0	27,3	1,87
Average	42,6	29,3	1,46	42,03	23,6	1,73

During dry weather periods minimum and maximum flows and depths of channels were specified from October 2011 to July 2012. The results are shown in Tables 1 and 2. For a detailed analysis 19 days when there was no rainfall were selected for position Skargi 1.1 and 27 for position Skargi 1.2. For each day minimum, maximum and average flow rate were specified. Based on the maximum and average values, peaking factors were estimated. The values of flow rates and peaking factors were shown in Table 3.

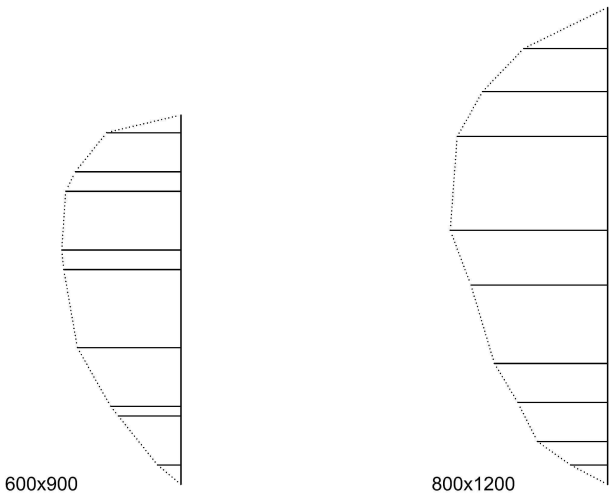

Fig. 4. Cross sections of channels reconstructed during the inventory

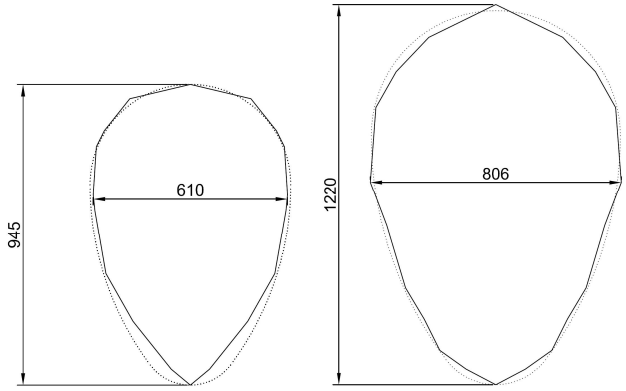

Fig. 5. Cross sections of channels reconstructed and typical

Flow rates in channels were estimated when depth is less then 20 cm and when it is not possible to perform measurements with the ultrasound probe. Obtained results are inadequate to real flow conditions. Flowmeter are located at a distance of less than 80 m. Therefore, the values obtained should be almost identical. As a reason, inadequate reconstruction of cross-sectional shape of the channel during device configuration was pointed (Fig. 4 and 5). This effect connected with low efficiency of the algorithm allows the estimation of the flow when depth is less then 20 cm (mistakenly called by the device manufacturer "Manning's formula method") is the cause of getting inconsistent results.

Tab 4. Dry weather peaking factors estimation – corrected values

Date	Flow rates – Skargi 1.1			Flow rates – Skargi 1.2		
	maximum	average	peaking factor	maximum	average	peaking factor
14.10.2011	50,5	37,8	1,34	53,0	41,6	1,28
16.10.2011	44,8	33,1	1,35	61,7	40,1	1,54
29.10.2011	44,2	33,8	1,31	54,0	41,0	1,32
31.10.2011	44,8	32,1	1,39	53,0	39,4	1,35
05.11.2011	45,4	34,4	1,32	54,0	41,5	1,30
15.11.2011	44,2	31,6	1,40	52,6	37,2	1,41
27.11.2011	42,4	31,4	1,35	54,0	39,0	1,38
29.11.2011	50,5	31,0	1,63	69,8	37,3	1,87
26.12.2011	46,0	32,8	1,40	55,5	38,2	1,45
31.01.2012	46,7	33,2	1,41	59,6	42,3	1,41
04.02.2012	44,2	33,0	1,34	69,2	44,0	1,57
07.02.2012	44,8	32,0	1,40	55,5	41,8	1,74
20.02.2012	-	-	-	53,5	37,9	1,41
02.03.2012	-	-	-	61,1	46,8	1,31
03.03.2012	-	-	-	72,6	49,5	1,47
04.03.2012	-	-	-	64,3	47,6	1,35
05.03.2012	-	-	-	60,6	46,4	1,31
07.03.2012	-	-	-	65,4	46,0	1,42
15.03.2012	-	-	-	64,3	44,2	1,45
20.03.2012	-	-	-	62,2	43,4	1,43
01.04.2012	48,8	35,9	1,39	56,5	40,8	1,39
11.04.2012	48,6	34,2	1,42	64,3	39,5	1,63
02.06.2012	47,9	34,9	1,37	65,4	42,5	1,54
24.07.2012	55,1	42,0	1,31	64,8	50,5	1,28
25.07.2012	56,4	41,1	1,37	64,3	49,2	1,31
26.07.2012	54,4	40,2	1,35	62,7	48,1	1,30
27.07.2012	64,8	41,1	1,58	80,8	49,4	1,63
Average	48,6	35,0	1,39	61,3	43,2	1,43

The results of corrective calculations based on Manning's formula and typical cross-sections of channels were presented in Table 4.

3. RESULTS ANALYSIS

Used measuring system was designed for storm water flows and combined overflows monitoring. ISCO ultrasonic profiling flowmeters measuring range starts at 110 mm, but in real technical conditions profiling starts at 200 mm. Dry weather flows connected with small depths are estimated with algorithms automatically adapting to changing hydraulic conditions within the pipe.

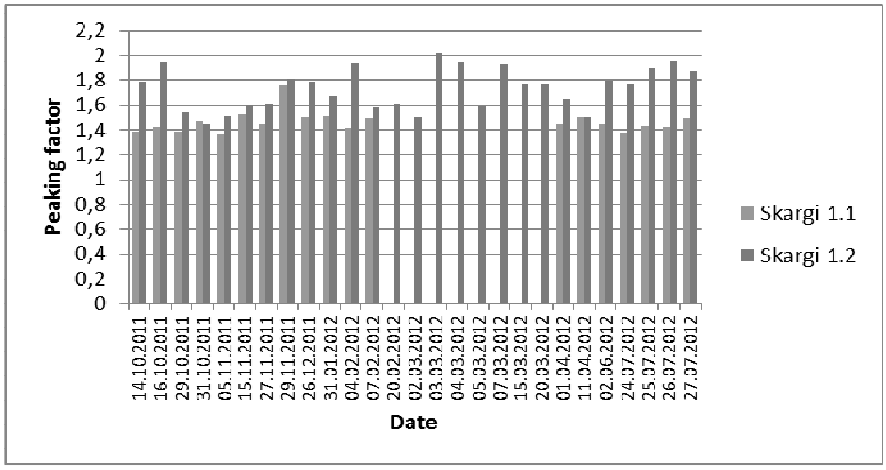

Fig. 6. Dry weather peaking factors – original values

Obtained results are inadequate to real conditions. Peaking factors estimated using logged data are characterized by significant differences between the two positions. In most cases the error exceeds 10% and in seven cases exceeds even 25%. Average peaking factor on Skargi 1.1 position is equal to 1,46. Average peaking factor on Skargi 1.2 position is equal to 1,73.

Peaking factors values calculated using corrected data are estimated with less error between the two positions. In most cases the error is less then 10%, only two cases exceeds 15%. Average peaking factor on Skargi 1.1 position is equal to 1,39. Average peaking factor on Skargi 1.2 position is equal to 1,44.
In cities the size of Głogów daily peaking factor is assumed of 1.4 (Gruszecki, Wartalski 1986).

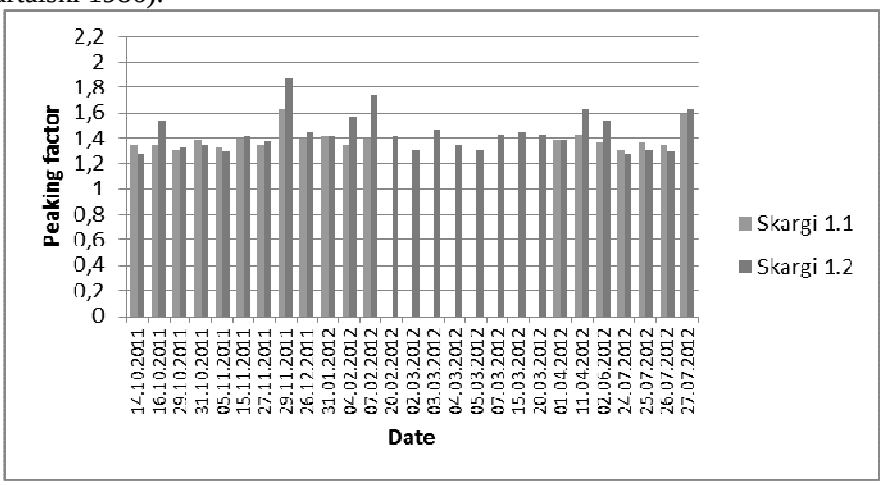

Fig. 6. Dry weather peaking factors – corrected values

4. CONCLUSIONS

Obtained results of corrected dry weather peaking factor are almost identical to typical designing factor. Original values are useless because of low efficiency of the implemented algorithms. An additional problem is limited experience of workers who build and implement measurement systems. Using profiling flowmeters to estimate dry weather values is not possible without manual calibration or correction values with Manning's formula. Optimal, though expensive solution is to apply additional ultrasonic flowmeter for small depths.

The calculations will be continued using the data obtained from measurements of the following years.

REFERENCES

1. Gruszecki T., Wartalski J.: *Kanalizacja*, Koszalin, Wydawnictwo Uczelniane WSI w Koszalinie, 1986.
2. Moulton R.B.: *Peaking factors in sanitary sewer design*, Brigham Young University, Provo, Utah 1999.

WSPÓŁCZYNNIK NIERÓWNOMIERNOŚCI PRZEPŁYWU POGODY BEZDESZCZOWEJ W KANALIZACJI OGÓLNOSPŁAWNEJ GŁOGOWA

S t r e s z c z e n i e

W pracy przedstawiono wyniki badań natężenia przepływu ścieków pogody suchej w kanałach dopływowym i odpływowym z przelewu burzowego PB-1. Obiekt zlokalizowany jest przy ulicy P. Skargi w Głogowie. W oparciu o uzyskane wyniki oszacowano średni współczynnik dobowej nierównomierności odpływu ścieków pogody bezdeszczowej. Stwierdzono niską efektywność algorytmu umożliwiającego szacowanie natężenia przepływu w zakresie 0-20 cm napełnienia kanału, gdy nie jest możliwe wykonywanie pomiarów przy użyciu sondy ultradźwiekowej. Wskazano na mało dokładne odtworzenie przekroju kanału w czasie konfiguracji urządzeń jako przyczyny uzyskiwania sprzecznych wyników pomiarów. Zaprezentowano wyniki obliczeń korygujących wykonane w oparciu o wzór Manninga i typowe przekroje kanałów. Uzyskane rezultaty potwierdzają możliwość wystąpienia znaczących różnic uzyskiwanych przy nieprawidłowo skonfigurowanych parametrach kanału. Potwierdzono niską jakość wbudowanego algorytmu wspomagającego pomiary przy małych napełnieniach, błędnie nazywanego przez producenta urządzenia metodą Manninga.

CIVIL AND ENVIRONMENTAL ENGINEERING REPORTS

No. 8 2012

WATER SUPPLY SYSTEM IN MIĘDZYCHÓD COMMUNE

Ewa OGIOŁDA[1*], Ireneusz NOWOGOŃSKI[1], Beata LESZCZYŃSKA
[1]University of Zielona Góra, Faculty of Civil and Environmental Engineering,
Institute of Environmental Engineering
Szafrana st 15, 65-516 Zielona Góra, Poland
FMT "Christianapol" Ltd. Łowyń

The properly designed and exploited water supply system is very important both for consumers and management in commune. Work conditions of such systems are changing so it is necessary to know its current parameters. Now we have different modern programs which make possible to calculate parameters and carry out simulation of designed changes which could improve reliability coefficients. Evaluation of exploited water supply system in Międzychód and designed its connection with subsystem in Radgoszcz were presented in this paper.

Keywords: water supply system, hydraulic calculations, numerical simulation

1. INTRODUCTION

Water supply systems are expensive while requirements for technical systems are higher and higher, so they are designed assuming their longlasting exploitation. One should create more durable and reliable systems. In properly designed system there should be realized distribution of required amount of good quality water under adequate pressure at the right time for consumers.

With passage of exploitation time work parameters are changing. There are software such as Epanet which makes possible to carry out calculations of existing systems or simulation calculations which let to estimate results of designed sytem changes.

* Corresponding author. E-mail: e.ogiolda@iis.uz.zgora.pl

2. CHARACTERISTIC OF WATER SUPPLY SYSTEM IN MIĘDZYCHÓD

City and commune Międzychód are localised on the Warta River, near the west boundary of Wielkopolskie Provence. There live about 6 thousand people in the city and about 12 thousand in commune Międzychód. There are great forest area and more than 50 lakes in the commune so during the summer there arrive many tourists – as a consequence water comsumption is very different, especially during a year [Studium uwarunkowań, 2005].

Fig. 1. Map of Międzychód commune [www.miedzychod.pl]

Most consumers in Międzychód commune has access to water distribution system, 17 from 26 villages are equipped with water pipe network. Technical condition of pipe system in a part of villages is poor [Plan zagospodarowania, 2007].

Tab. 1. Specification of water supply subsystems [ZGKiM Międzychód, 2009]

Lp.	Subsystem	Villages	Number of consumers
1	Międzychód	Międzychód, Bielsko, Dzięcielin, Wielowieś, Zatom Stary, Kolno, Muchocin, Gorzycko Stare, Gorzyń	14.776

2	Radgoszcz	Radgoszcz, Mierzyn, Przedlesie, Kaplin, Zwierzyniec, Mokrzec, Zatom Nowy, Puszcza	1.165
3	Kamionna	Kamionna, Mocberk – Folwark	516
4	Głażewo	Głażewo, Skrzydlewo, Gralewo, Dormowo, Mnichy, Mniszki, Tuczępy	1.196
5	Lewice	Lewice	219
6	Łowyń	Łowyń	716

3. CALCULATION METHOD

Hydraulic calculations were computed with EPANET 2 prepared by The National Risk Management Research Laboratory. This program is applied in water ditribution system analysis, makes possible analysis of water flow, pressure values in particular nodes, water level in tanks and reservoirs and concentration of chemical compounds in pipes. Obtained results are presented in different forms – tables, graphs, contour plots, profiles what allows to evaluate changes designed in water network [Rossman, 2000].

Input data necessary in hydraulic model of water network are:

- grahical presentation of pipe network,
- lengths, diameters and roughness coefficients of pipes,
- water demands in nodes,
- localisation of reservoirs, tanks and pump stations.

The hydraulic headloss by water flowing in a pipe can be computed using one of three different methods:

- Hazen-Williams formula,
- Darcy-Weisbach formula,
- Chezy-Manning formula.

In carried calculation Darcy – Weisbach formula was chosen [Rossman, 2000]:

$$\Delta h_L = Aq^B$$

where: Δh_L - headloss, m,
q - flow rate, m^3s^{-1}
B - flow exponent, B = 2,

A - resistance coefficient,

$$A = 0.0252\ f(\varepsilon,d,q)\ d^{-5}L$$

ε – Darcy – Weisbach roughness coefficient, mm,
d – pipe diameter, m,
L – pipe length, m.

4. CALCULATIONS OF EXPLOITED PIPE NETWORK

Existing pipe network consists of 9 loops and pipes of total length 88 km. Elevations on Międzychód commune area are significantly differentiated - about 32,5 m so this is necessary to apply a few pump stations. Diameters of pipes ranges from 90 to 250 mm. Graphical representation of water pipe network in Międzychód is shown in figure 2.

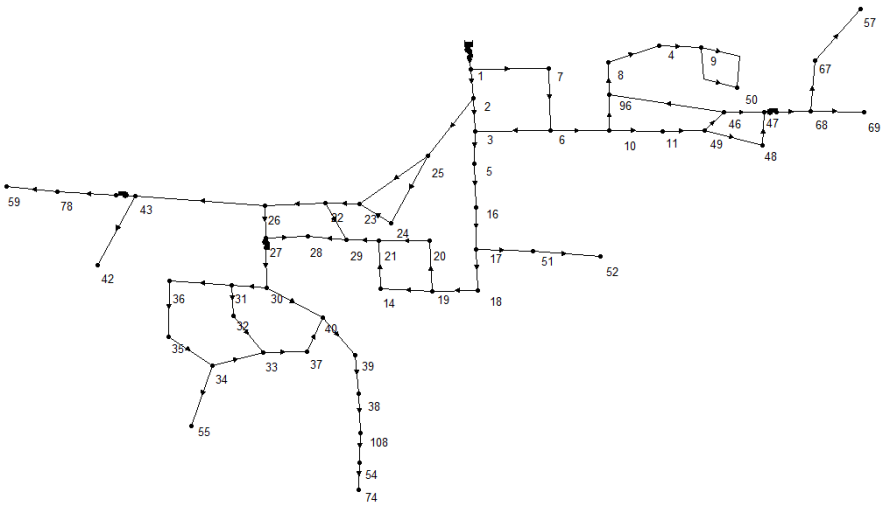

Fig. 2. Graphical representation of water pipe network in Międzychód

Calculations were realized in terms of real consumption - water demand was evaluated for number of consumers established as it is shown in tab. 1. Maximum singular coefficient of water consumption was accepted as an average value from 2006 – 2008 – it means $q = 90\ dm^3 \cdot M^{-1} \cdot d^{-1}$.

The results of carried out calculations make possible to evaluate work conditions in exploited water distribution system. As the results one obtaine values of pressure and flow velocity (tab.2).

Tab. 2. Zakresy prędkości przepływu i ciśnienia w systemie Międzychód

Parameter	Minimum value	Maximum value
Water pressure [m]	23,77	61,77
Flow velocity [mps]	0,11	0,73

Results were shown on contour plot – ranges of pressure in particular nodes (fig. 3).

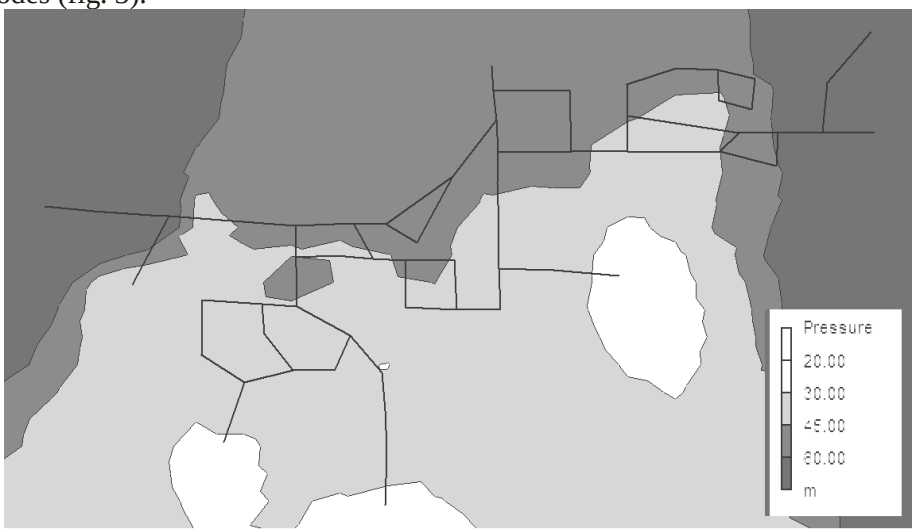

Fig. 3. Contour plot of pressure in system of Miedzychod commune

Results show that pipe network is exploited under too high pressure, not adjusted to real needs, however maximum pressure exceeds allowed 60 m only outside of supply area. Flow velocity values in many pipes are too low - minimum value 0,5 $m \cdot s^{-1}$ was achieved only in 20% of pipes length.

Parameters differ from those which should be guaranteed during correct explotation what is the result of water demand decrease.

5. NUMERICAL SIMULATION OF CONNECTED WATER SUBSYSTEMS

To improve reliability connection of two subsystems Międzychód and Radgoszcz was considered. Elevation in both cases are similar and in case of breakdown of one water treatment station there is a possibility to distribute water from other. Capacity of water intake in Międzychód equals to 175 $m^3 \cdot h^{-1}$, so it is sufficient to meet water demand for Międzychód and Radgoszcz. On the other hand intake capacity in Radgoszcz is 35 $m^3 \cdot h^{-1}$, so it could ensure only about 20% of water requirements for Międzychód. Connection was designed in node 22 and simulation was carried out for pipe of diameter Ø300 under conditions of maximum demand of water.

Graphical representation of connected subsystems Międzychód and Radgoszcz is shown in fig. 4.

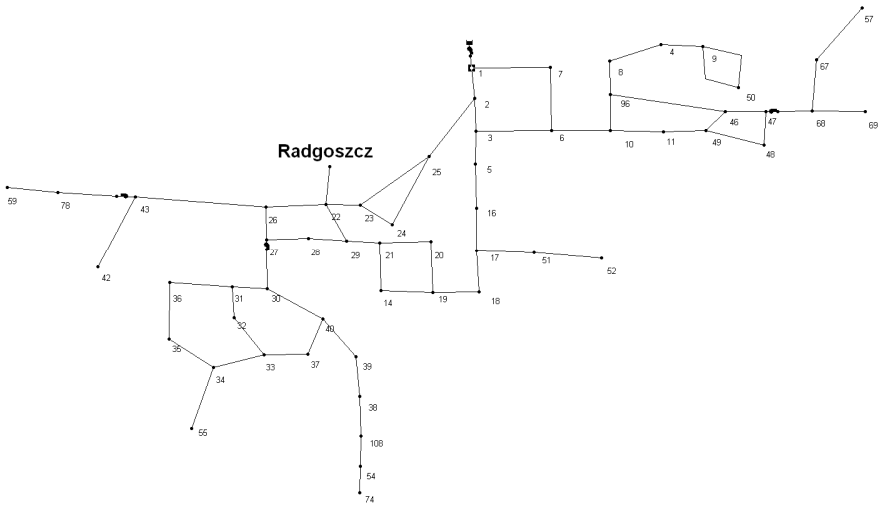

Fig.4. Graphical representation of connected subsysterms Międzychód and Ragdgoszcz

Tab. 3. Velocity and pressure ranges in connected subsystems

Parameter	Minimum value	Maximum value
Water pressure [m]	15,66	50,66
Flow velocity [mps]	0,01	1,00

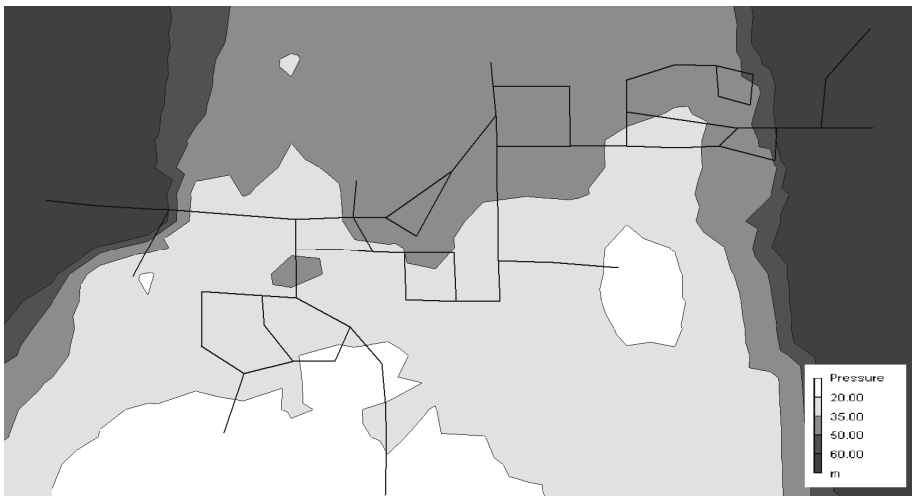

Fig. 5. Contour plot of pressure in connected subsystems Międzychód and Radgoszcz

Obtained simulation results show that it is possible to connect water system supplied from water treatment station in Radgoszcz to subsystem in

Międzychód. Pressure range is sufficient for low buildings which are typical of village area, but flow velocity values are lower than 0,5 $m \cdot s^{-1}$, so it is necessary to rinse pipe network.

6. CONCLUSIONS

Evaluation of exploited system should be the base of taking decisions concerning the best solutions choise in respect of the technical, economical and reliability point of view at a stage of design, realization and exploitation.

Results of carried calculations make possible to evaluate existing water supply system in Międzychód. Analysis confirms by low values of flow velocity that pipes diameters are too large. It could result in deterioration of physical, chemical and bacteriological water quality. System supply under exscessive pressure could cause breakdowns and increased water losses.

Results show correctness of reliability improvement by application of subsystems additional connection. Carried out simulation of connected subsystems Międzychód and Radgoszcz proves that it ensures better reliability of water deliverying to consumers both during standard exploitation and in case of increased demands (e.g. extinguishing fire).

Water supply system in Międzychód should be modernized, especially in regards pipe diameters and extension pipe network by connection with other subsystems. Prepared hydraulic model makes possible to simulate and evaluate introduced in future changes.

REFERENCES

1. Rossman L.A.: *Epanet 2. User's Manual*, Cincinnati 2000
2. Miejscowy plan zagospodarowania przestrzennego miasta Międzychód oraz obrębów: Bielsko, Dzięcielin, Wielowieś oraz części obrębu Muchocin 2007 r.
3. Studium uwarunkowań i kierunków zagospodarowania przestrzennego gminy Międzychód 2005 r.
4. Zestawienie zużycia wody, ZGKiM Międzychód 2009

SYSTEM ZAOPATRZENIA W WODĘ W GMINIE MIĘDZYCHÓD

S t r e s z c z e n i e

Systemy zaopatrzenia w wodę są kosztownymi inwestycjami – isotne jest zatem z punktu widzenia użytkowników projektowanie i eksploatowanie ich w taki sposób, aby pracowały niezawodnie przez długi czas. Warunki pracy omawianych systemów zmieniają się w czasie ich użytkowania – istotna jest zatem znajomość aktualnych wartości poszczególnych parametrów eksploatacyjnych. Cennymi narzędziami są programy komputerowe, które umożliwiają zarówno ustalenie wartości poszczególnych parametrów, jak i przeprowadzenie obliczeń symulacyjnych dla projektowanych w systemie zmian mających przyczynić się do poprawy jego niezawodności. Przy użyciu programu EPANET obliczono i poddano analizie parametry pracy istniejącego systemu zaopatrzenia w wodę w Międzychodzie. Zaproponowano połączenie systemu z podsystemem Radgoszcz, a uzasadnieniem prawidłowości takiego rozwiązania są wyniki przeprowadzonych obliczeń symulacyjnych.

CIVIL AND ENVIRONMENTAL ENGINEERING REPORTS

No. 8 2012

THE COMPLEXES OF ANTIBIOTICS WITH TRACE METALS

Marlena PIONTEK, Zuzanna FEDYCZAK, Katarzyna ŁUSZCZYŃSKA*
University of Zielona Góra, Faculty of Civil and Environmental Engineering,
Institute of Environmental Engineering
Szafrana st 15, 65-516 Zielona Góra, Poland

This article, basing on the available literature, summarizes the results of physiochemical research into the structure of complexes of trace metals with antibiotics. It presents the leading methods of instrumental analysis applied to determine the structure of complexes.

Keywords: ntibiotics, trace metals, complexes of trace metals, instrumental analysis

1. INTRODUCTION

The term antibiotics [Gr. *anti* - against, *bios* - life] refers to a group of organic natural chemical compounds produced by such microorganisms as: bacteria, actinobacteria, warious types of fungi and some plants and animal cells. Many substances isolated from these organisms are synthesized on an industrial scale as a whole (of synthetic origin, called chemiotherapeutics) or in part (of semisynthetic origin), [16]. The products of metabolism of actinobacteria constitute about 90% of natural antibiotics produced on an industrial scale [5].

The research into moulds has enabled the acquisition and consequently the synthesis and modification of the acquired compounds although their role in the life of microorganisms has not been explained [5]. From the medical point of view some of the most important metabolites secreted by the *Penicilium chrysogenum* Thom mould are penicillin G. and griseofulvin. Yet many other metabolites also have a wide range of action: antiseptic against *Staphylococcus aureus*, decomposing carbohydrates, oxidizing decanes, undecanes and hexadecanes from petroleum. The *Acremonium strictum* W.Gams mould

* Corresponding author. E-mail: k.luszczynska@iis.uz.zgora.pl

produces cephalosporin, which has become the source compound for five generations and over 20 various derivatives of cephalosporins and the *Thamnidium elegans* Link mould produces an antibiotic inhibiting the development of mycobacteria [10]. A common feature of all antibiotics and chemiotherapeutics is their ability to inhibit the metabolism and multiplication - the basic life processes - of microorganisms.

The biosynthesis of antibiotics is based on several starting substances and depends on the environmental conditions. With both *Penicilium chrysogenum* and *Acremonium strictum* the substrates are acetyl-CoA, acetylserine, L-methionine, pyruvate, and 2-oxoglutarate of the Krebs cycle. These compounds are converted to three amino acids and subsequently to a tripeptide, which, as a result of enzyme action, produces the intermediate isopenicillin N. The *Penicilium* moulds convert it to penicillins, whereas the *Acremonium* moulds convert it to cephalosporins and cephamycins [5].

The growing drug resistance of microorganisms has resulted in the rapid development of pharmacology and chemistry. A lot of antibiotics have been found, which have been divided according to their chemical structure and the range of effect on microorganisms. With regard to structure the following can be identified: beta-lactams (penicillins, cephalosporins, monobactams, carbapenems, beta-lactamese inhibitors), tetracyclines, quinolones, aminoglycosides, peptide antibiotics, sulfonamides, linkosamides, chloramphenicol, macrolides, ansamycins.

Some of these groups turned out to be promising due to the possibility of synthesizing derivatives whose properties are stronger than those of the source substances, and which are more active, more water-soluble, more lasting, of better therapeutic index, broader application and limited adverse drug reaction.

Antibiotics differ from one another in terms of the way they effect microorganisms. Two mechanisms are, however, prevalent. One of them is based on the destruction or prevention of the production of the cell wall, which consequently leads to the loss of its contents by the cell. The other mechanism consists in the blocking of metabolic pathways by antibiotics - the inhibition of the process of creating proteins prevents the cell from developing and regenerating properly. The physiochemical properties vary and depend on a number of factors, such as pH, the functional groups in a molecule and its general structure [16].

Trace metals are elements including copper, manganese, iron, vanadium (or more precisely - vanadyl - VO^{2+}), chromium, zinc and cobalt. They are essential to the proper functioning of the organism. Their daily demand does not exceed 100 mg and their excess may cause numerous and serious side effects. The role of trace metals is most frequently to regulate metabolism because many of them constitute the important part of enzymes (zinc, molybdenum) or

vitamins (cobalt). They enable cellular respiration by supplying oxygen to tissues and cells (iron), are involved in the synthesis of neurotransmitters (copper) and protect from free radicals (manganese), [7]. Pure trace metals are toxic for the organism [8]. However, they enter the organism from food as complex compounds [7,12].

Many of the chemical compounds come in contact with antibiotics in human body, among them ions of trace metals. Effects of their synthesis can be harmful, neutral or curative and is dependent on their solubility, assimilation, polarity and chemical structure. Getting to know of that structure may be key to predicting the behavior of these substances in the organism, or even finding new ways of their usage. Knowing the most efficient methods of analyzing complex compounds will allow us to quickly and inexpensively research their previously mentioned attributes, witch in turn may be helpful in synthesizing next generation, more efficient and selective medicaments.

The purpose of this paper is to determine, based on literature data, the most efficient methods of identification of antibiotics-trace metals complexes.

2. RESEARCH METHODOLOGY REVIEW

The applied methodology consisted in the analyzing and comparing of the most frequently performed spectra and characteristic parameters of free antibiotics and their complexes with trace metals. The most frequently used methods were the following: the IR (infrared spectroscopy), UV-Vis (Ultraviolet-visible spectroscopy) spectrophotometry, ^{1}H NMR (Proton Nuclear Magnetic Resonance) and ^{13}C NMR (Carbon-13 Nuclear Magnetic Resonance) spectrometry, polarography, molecular modelling, crystallographic measurements, EXAFS (Extended X-Ray Absorption Fine Structure), mass spectrometry, EPR (Electron Paramagnetic Resonance) and the measurements of the magnetic moment [2, 3, 4, 11, 13].

3. ANALYSIS AND EVALUATION OF APPLIED METHODS' USEFULNESS

The IR spectrum of trace metal complexes with penicillins provides valuable information. The study of the presence of signals of free penicillin G and ampicillin and their complexes with copper allows one to clearly determine which functional groups are engaged in the coordinate bond. Table 1 confirms the research data. The lack of signal typical of lactam group testifies to the hydrolysis of the lactam ring, namely the decomposition of penicillin into the penicillic acid (Figure 1).

Table.1. IR spectrum data for benzilpenicillin (PenG) i ampicillin (Amp) and their binding with Cu(II) G* and Amp* stands for ligand of penicillic acid [13]

Functional group	ν [cm^{-1}] for PenG	ν [cm^{-1}] for $Cu(PenG)_2$	ν [cm^{-1}] for Amp	ν [cm^{-1}] for $Cu(Amp)_2$
C=O (lactam)	1780	no spectrum	1780	no spectrum
C=O (amide)	1680	1660	1680	1660

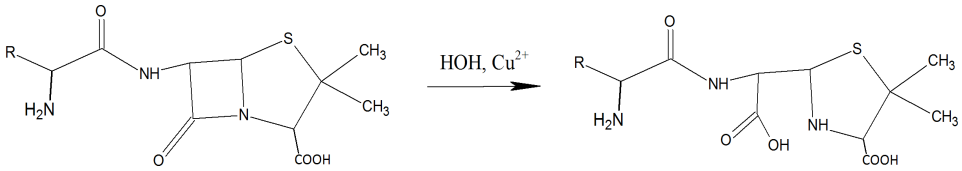

Fig. 1. Hydrolysis of penicillins to penicillic acid in the environment of copper ions [13]

The spectrophotometric study (UV-Vis) of penicillin solutions confirms their coordinative properties (Figure 2). For 1:1 solutions (ligand:metal) the maximum absorption is observed at 715-755 nm; with a portion of the ligand added to the solution the maximum is found at 318-366 nm (Figure 2). This is due to the precipitated sludge and confirms the creation of a new compound containing more ligands bound with the coordination centre. The minimum absorption for the compound is observed at 2:1 ligand:metal ratio [13].

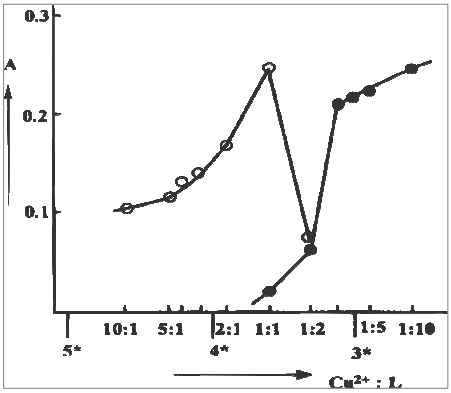

Fig. 2. Absorbance dependence for the copper-penicillin G complex for specific stoichiometric ratios. ● for λ 318 nm, ○ for λ 755 nm [13]

Cephalosporins create complexes at various stoichiometric ratios, and the ligand co-ordinates the metal ion through various donor groups depending on pH. It all results closely from the molecule structure [4]. The study of the bonding of cefadroxil with metal ions has provided a lot of important information. These complexes are stable - as proved by the log K value (= 6 – 13) oraz ΔG (= 8.5 – 18.5 kcal/ mol·K). The IR spectrum of cefadroxil includes

a band at 1354 cm^{-1} attributed to the stretching vibrations of the C-N beta-lactam ring and the thiazolidine ring. There is no such band in the spectrum of the complexes, which indicates the participation of nitrogen atoms of these rings in the coordinate bond (Figure 3). The stretching vibrations of the C-O group coming from the beta-lactam ring of the cefadroxil molecule, which occur at 1759 cm^{-1}, are not found in the complex spectrum (Table 2). This is evidence of this group being engaged in the chelation of the metal ions. In the spectrum of the complex the bands for symmetrical stretching vibrations (COO) are shifted towards higher frequencies by about 30-50 cm^{-1} as compared with the spectrum of free cefadroxil. This points to the participation of the carboxyl group in the coordinate bond. Studies have also shown that the amide group is not engaged in the creation of the complex as its band does not undergo shifting [15].

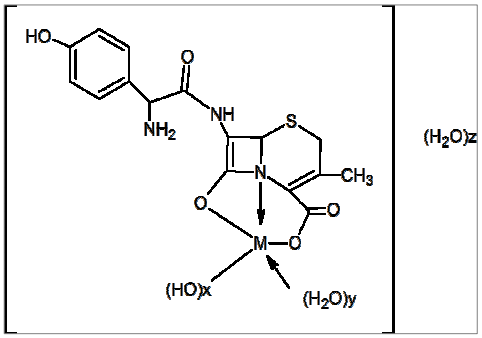

Fig. 3. The general structure of the cefadroxil-trace metal complex, where M stands for Fe(II) x=0 y=1 z=2,Ni(II) and Cu(II) x=1 y=0 z=1 [15]

Table 2. Selected bands of the IR spectrum attributed to cefadroxil and their complexes (L-ligand cefadroxil) within the wavelength of 4000-200 cm^{-1} [15]

Complex	ν (C-N) in the ring in [cm^{-1}]	ν (C=O) in the ring in [cm^{-1}]	ν_{sym} (COO) in [cm^{-1}]
[Fe(II) L(H_2O)] ·2H_2O	no band	no band	1261
[Ni(II)L(OH)]·H_2O	no band	no band	1236
[Cu(II) L(OH)]· H_2O	no band	no band	1234

The properties of the cefaclor-copper (II) complex were studied by means of spectrophotometry with the pH value set and maintained at 8.0 with the use of a pH meter. Cefaclor may behave like an acid and a base at the same time. It may also be a zwitterion. In the acidic environment its complex with copper (II) hydrolyzes into $Cu(CEF)^{+}$, and in the slightly basic environment a hydrocomplex Cu(OH)(CEF) is created, which is confirmed by the study of pH values (Figure 4). With the pH value over 9.0 the absorbance increases and the maximum shifts towards longer wave lengths - the $Cu(OH)_2$(CEF) complex is

created. With the pH over 10.7 the colour of solution turns intensly into yellow and orange, which probably results from the decomposition of cefaclor in the strongly basic environment. It was supposed that copper catalyzes the hydrolysis of cefaclor, but this hypothesis was not confirmed. The obtained results agree with the assumption that the metal ion is not engaged in the stabilization of the tetraedric complex created with the opening of the lactam ring. That confirms the prediction that the copper ion co-creates a complex outside the ring at pH = 8.0.

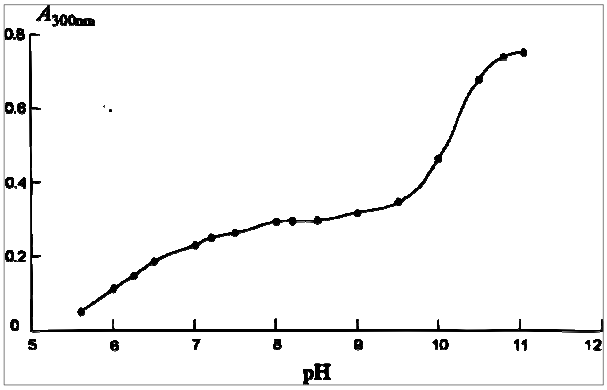

Fig. 4. Absorbance-pH dependence for the cefaclor-copper complex at 300 nm [3]

A UV-Vis spectrum was performed for the 400 - 282 nm range for copper salts (II), cefaclor and the complex of copper with cefaclor. For cefaclor the maximum absorption is found at 282 nm, whereas for the complex it occurred at 300 nm, which serves as confirmation of the creation of this complex (Figure 5), [3].

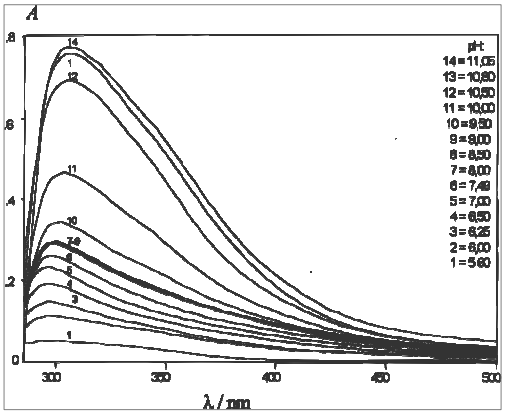

Fig. 5. The UV spectrum for the copper (II)-cefaclor complex in changing pH [3]

Aminoglycosides readily chelate metal ions, but for this to happen the condition must be met that there are four or more atoms of nitrogen (amine groups) present. Gentamicin includes 5 amine groups, only 3 of which have the capacity to coordinate, creating a 1:1 complex.

The ^1H NMR spectrum for the iron-gentamicin complex is a useful tool for analysing the structure of the compound (Figure 6).

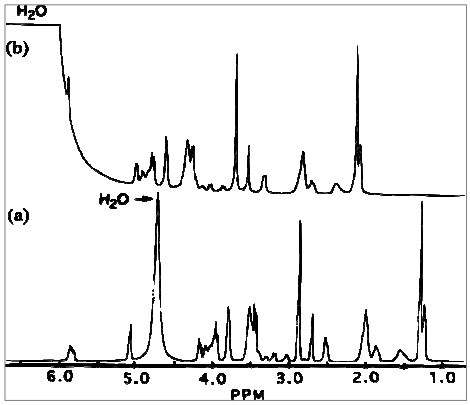

Fig. 6. The value of chemical shift for the complex (b) as compared with the free antibiotic (a) equals approx. 1 ppm [11]

It follows that the signal bandwidth in the spectrum of the complex approximates the signal bandwidth in the spectrum of free gentamicin. That has confirmed the hypothesis about the weak interaction of the ligand with the metal ion [11]. Molecular modelling indicates that the chelation of iron by one gentamicin molecule does not prevent attaching another gentamicin molecule. Hence, if there is a high concentration of the antibiotic, a 2:1 (antibiotic: metal ion) complex arises (Figure 7).

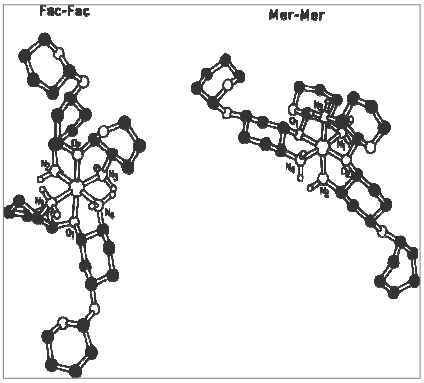

Fig. 7. Proposed structures for the 2:1 gentamicin:iron complex [11]

The research on aminoglycosides has shown that these antibiotics very effectively bind with copper (II) (kanamycin A even one hundred times as strongly as with other metals) in the environment of physiological pH [14]. Aminoglycosides are known for their oto-, hepato- and nephrotoxic effect on the human organism [16]. That may be caused by radicals, which appear in the presence of the complexes of these antibiotics with trace metals. Although these substances themselves do not have reduction-oxidation abilities and therefore require a special medium to participate in such processes, ions of transition metals Ni(II), Co(II), Zn(II) or Cu(II) seem to be ideally suited for that. Although the amount of 'free' copper in the human organism is quite small, during illness (tumour, inflammations) its levels increase and the creation of a complex becomes fully possible [14]. Peptide antibiotics have a great capacity to bind the ions of bivalent metals at the 1:1 ratio. It has been established that this affinity decreases in the series: $Cu^{2+} > Ni^{2+} > Co^{2+} \sim Zn^{2+} > Mn^{2+}$ [6]. It is thought that the bacitracin molecule chelates metal ions by means of the thiazolidine and imidazole ring of histidine. The engagement of the imidazole ring has been determined with the help of the ^{1}H NMR spectrum, on the basis of an equal shift of its value towards the lower range for both 2-CH and 4-CH and by analysing the ^{13}C NMR spectrum, at pH = 6-8. This theory needs confirmation by further studies. It has been established that the above-mentioned ions chelate with the sulphur atom of the thiazolidine ring and the carboxyl group of the glutamic acid (Figure 8). It follows from the EPR spectra that Mn^{2+} does not create complexes with the antibiotic below pH = 5.2. The Cu^{2+}- bacitracin complex, on the other hand, gives the EPR spectrum, which is consistent with the assumption that the complex has a distorted tetragonal geometry with two coordinated atoms of nitrogen and two atoms of oxygen. The EXAFS study indicates that in the coordination sphere of the metal there are three N-ligands and one ligand with an atom of oxygen, attributed most probably to the nitrogen of the terminal amine group of the imidazole ring of histidine, the thiazolidine nitrogen and the carboxyl group of the glutamic acid [6].

Many scientists have conducted research into the complexes of trace metals with quinolones because the presence of carboxyl and carbonyl groups ensures good chelation and the creation of relatively small compounds [16]. The proposed method of the complexation of metal ions postulates interaction between the 4-oxo and the neighbouring hydroxyl group, which are a constant and indispensable element ensuring that quinolone antibiotics have bacteriostatic abilities.

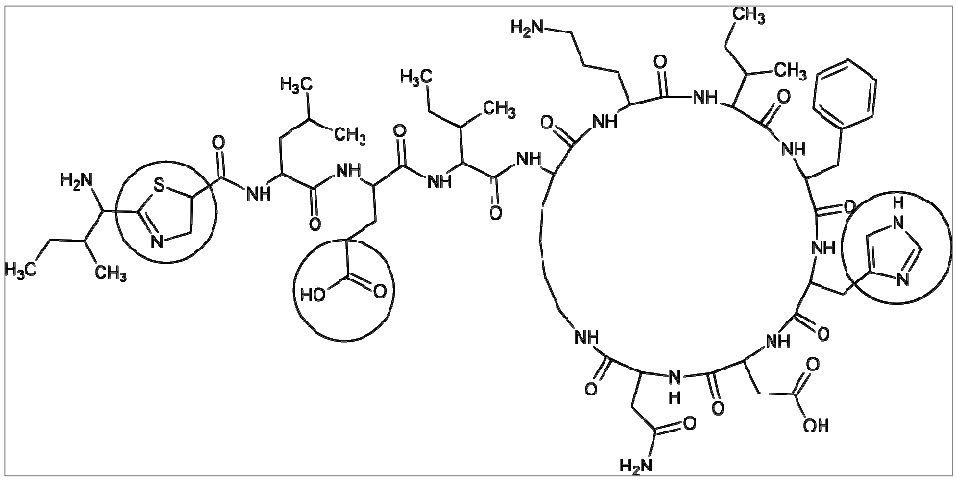

Fig. 8. Bacitracin with the groups engaged in the chelation of ions of trace metals [6]

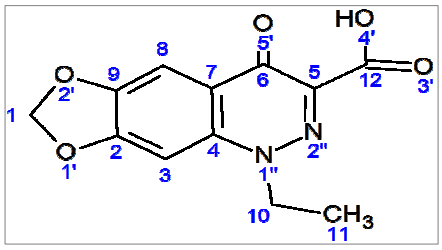

Fig. 9. Cinoxacin. The presence of the 5-oxo and carboxyl group ensures excellent chelating properties [16]

Another example that confirms the method of chelation of metal ions by quinolones is the complex $[Cu(hsm)(nal)H_2O]Cl \cdot 3H_2O$ (hsm - histamine, nal - nalidixic acid), in which one can observe d-d transitions at 625 nm, attributed to the complexes of square based pyramidal geometry including two coordinated nitrogen atoms. In the IR spectrum one can observe broad bands between 1634 and 1501 cm^{-1} attributed to the stretching vibrations including both the functional group COO and CO. It serves as further confirmation of the interaction between the metal ion and the carbonyl (5-oxo) and the carboxyl group within a molecule of this antibiotic (Figure 9), [1]. Another case confirming the structure of the complexes of metal ions with quinolones is the $[Cu(hsm)(cnx)NO_3] \cdot H_2O$ complex (where hsm stands for histamine, and cnx for cinoxacin - Drawing 4). It acquires the geometry of a distorted square based pyramid - the crystallographic analysis serves as confirmation (Figure 10, Tab. 3), [2].

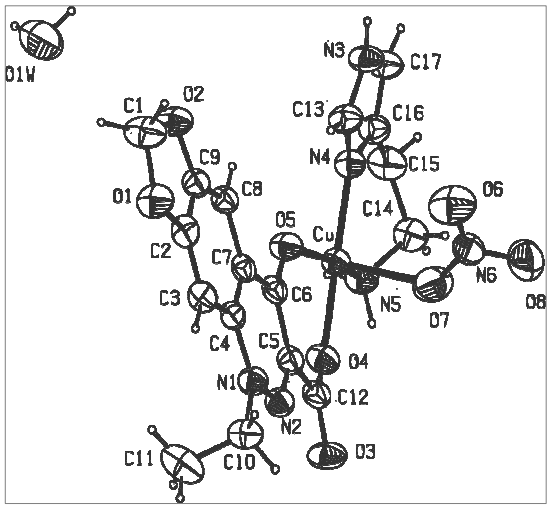

Fig. 10. The crystal structure of the complex with the particular atoms marked [Cu(hsm)(cnx)NO3] ·H2O [2]

Table 3: Comparison of bond length in free cinoxacin and its complex with copper (II) based upon crystallographic research [2]

Carbon bond in antibiotic	Bond length in free antibiotic	Bond length in complex of antibiotic	Type of change in bond
C(5) - C(6)	1.451	1.442	shortening
C(6) - O(5')	1.248	1.270	lengthening
C(12) - O(4')	1.316	1.269	shortening
C(5) - C(12)	1.503	1.511	lengthening

4. SUMMARY

In this study the most frequent methods of instrumental analysis applied to identify complexes of trace metals with antibiotics have been selected from the available literature and their accuracy has been compared. The methods used for identification and analyzing the results have been expounded with reference to particular groups of antibiotics. Also, available information has been collected on the physicochemical properties of the complexes. This knowledge is indispensable to make predictions about the behaviour of molecules in the organism and to create new, lasting and effective antibiotics.

Each method of analysis has it's pros and cons. In IR and UV-Vis spectroscopy the ease of sample preparation, result interpretation and inexpensive procedure is offset by the fact that not all substancs can be

examined. The EPR method only allows the study of trace metals with unpaired electrons. ^{1}H NMR and ^{13}C NMR methods are costly, altough they provide useful information about structure.

In case of complicated structure compounds mass spectrometry defines their mass but is otherwise difficult to interpret. The EXAFS method does not give sufficient information about the structure, and is only limited to defining distance between atoms, furthermore it is used to examine amorphic materials. Polarography provides information about ion stability and concentration, but it is hazardous for scientists' health, there is a possibility of sample contamination and interferation with electrolytes. Cristallographic analysis are costly, the studies themselves are time consuming and in case of complicated structure compounds is difficult to interpret. Howevere it provides us with greatest amount of information about examined substance structure.

Each of the presented methods has in its own way confirmed or negated the hypothetical structure of the complex. The preferred method was IR and UV-Vis spectroscopy. It is most probably due to the ease it ensures in preparing the results and the relatively low cost of measurements as compared with f. ex. EPR, polarography or magnetic methods.

5. CONCLUSIONS

This study, based on the literature data, summarizes the results of physiochemical research on the structure of complexes of trace metals with antibiotics. These compounds have been studied with nearly all known groups of antibiotics as they contain heteroatoms and as such have excellent donor properties. Their structure is not always easy to interpret. No single method allows us to clearly specify the structure of the examined compound. Using multiple analysis methods gives better results. Spectroscopic and crystallographic methods are prefered by scientists. The knowledge of a structure, the methods of its synthesis and its effect on the human organism allows for the creation of a new class of substances. Its extended effect on microorganisms may result in their reduced drug resistance.

REFERENCES

1. Bivian-Castro E.Y., Lopez M.G.: *Synthesis, characterization, and biological activity studies of copper(II) mixed compound with histamine and nalidixic acid.* Bioinorganic Chemistry and Applications (2009) 4-6.
2. Bivian-Castro E.Y., Cervantes-Lee F.: *Synthesis, characterization and crystal structure of copper(II) ternary complex with cinoxacin and histamine*. Inorganica Chimica Acta, **357** (2004) 349-353.

3. Dimitrovska A., Andonovski B.: *Spectrophotometric study of copper(II) ion complexes with cefaclor*. International Journal of Pharmaceutics, **134** (1996) 213-221.
4. El-Maali N.A., Osman A.H.: *Voltammetric analysis of Cu (II), Cd (II) and Zn (II) complexes and their cyclic voltammetry with several cephalosporin antibiotics*. Bioelectrochemistry, **65** (2005) 95-104.
5. Libudzisz Z., Kowal K. [praca zbior.]: *Mikrobiologia techniczna*. T.2. Łódź, Wyd. Politechniki Łódzkiej, 2000.
6. Ming L.J., Epperson J.D.: *Metal binding and structure–activity relationship of the metalloantibiotic peptide bacitracin*. Journal of Inorganic Biochemistry, **91 (**2002) 46-58.
7. Murray R., Granner D.K.: *Biochemia Harpera Ilustrowana*, Warszawa, Wyd. PZWL, 2006, 601-606.
8. Murray R., Granner D.K.: *Biochemia Harpera*. Warszawa, Wyd. PZWL, 1995, 730-731.
9. Piontek M.: *Grzyby pleśniowe i ocena zagrożenia mikotoksycznego w budownictwie mieszkaniowym*. Zielona Góra, Oficyna Wyd. Uniwersytetu Zielonogórskiego, 2004.
10. Piontek M.: *Atlas – Grzyby pleśniowe*. Wyd. Politechniki Zielonogórskiej, Zielona Góra, 1999.
11. Priuska E.M., Clark-Baldwin K.: *NMR studies of iron-gentamicin complexes and the implications for aminoglycoside toxicity*. Inorganica Chimica Acta , **273** (1998) 85-91.
12. Seńczuk W.: *Toksykologia współczesna*. Warszawa, Wyd. PZWL, 2006.
13. Sher A., Veber M.: *Spectroscopic and polarographic investigations: Copper(II) - penicillin derivatives*. International Journal of Pharmaceutics, **148** (1997)191-199.
14. Szczepanik W., Kaczmarek P.: *Oxidative activity of copper(II) complexes with aminoglycoside antibiotics as implication to the toxicity of these drugs.* Bioinorganic Chemistry and Applications. **2**, 1-2 (2004) 55-68.
15. Zayed M.A., Abdallah S.M.: *Synthesis, characterization and electronic spectra of cefadroxil complexes of d-block elements*. Spectrochimica Acta Part A: Molecular and Biomolecular Spectroscopy **60** (2004) 2215-2224.
16. Zejc A., Gorczyca M.: *Chemia leków*. Warszawa, Wyd. PZWL, 2004.

KOMPLEKSY ANTYBIOTYKÓW Z METALAMI ŚLADOWYMI

S t r e s z c z e n i e

W artykule, na podstawie danych pochodzących z pismiennictwa, zestawiono wyniki badań fizykochemicznych nad strukturą kompleksów antybiotyków z metalami śladowymi. Przedstawiono wiodące metody analizy instrumentalnej służące do określania struktury kompleksów.

Słowa kluczowe: antybiotyki, metale śladowe, kompleksy metali śladowych, analiza instrumentalna

CIVIL AND ENVIRONMENTAL ENGINEERING REPORTS

No. 8 2012

TWO-DIMENSIONAL HEAT CONDUCTION IN THE LAMINATE WITH THE FUNCTIONALLY GRADED PROPERTIES

Alina RADZIKOWSKA*, Artur WIROWSKI*
Department of Structural Mechanics,
Technical University of Łódź,
Al. Politechniki 6, 90-924 Łódź, Poland

The object of the contribution is the classical Fourier heat conduction in the laminate with functionally graded properties. The laminate is made of two conductors, non-periodically distributed as laminas along one direction. A macrostructure of the laminate is assumed to be functionally graded along this direction. In order to analyse heat conduction, the tolerance averaging technique is used. The approach is based on the book edited by Cz. Woźniak, Michalak and Jędrysiak [10] and by Cz. Woźniak et al. [6]. The aim of this paper is to apply the tolerance model equations of heat conduction for laminate with functionally graded properties to analyse two-dimensional stationary heat transfer. The equations of the tolerance model are solved by the finite difference method.

Keywords: heat conduction, functionally graded laminates, tolerance modelling.

1. INTRODUCTION

The main object under consideration is the laminate made of two conductors. These conductors are distributed non-periodically along the direction normal to the laminas. Every lamina has the thickness λ (λ is constant). It consists of two sublaminas (the thickness of each sublamina changes in every lamina). From the macroscopic point of view averaged (macroscopic) properties of this laminate are continuously varied along one direction, cf. Fig. 1a. However, the microstructure of the laminate can be defined by some distribution functions, which determine the thicknesses of sublaminas, cf. Fig. 1b.

* Corresponding author. E-mail: alina.radzikowska@p.lodz.pl, wirowski@p.lodz.pl

The laminates of this kind can be treated as made of the functionally graded materials (FGM), cf. Suresh and Mortensen [9].

There are many modelling techniques we can use to research thermo-mechanical problems of the functionally graded materials. One of them is the asymptotic homogenization. As an alternative approach, for FG-type materials the higher-order theory was proposed by Aboudi, Pindera and Arnold [1] and then with its reformulation by Bansal and Pindera [2]. In this paper we focus on the tolerance averaging technique (*the tolerance modelling*), extended on FG-type materials in books edited by Cz. Woźniak, Michalak and Jędrysiak [10] and by Cz. Woźniak et al. [6]. This technique was adopted to analyse various problems of FG-type materials and structures in series of papers, e.g. for heat conduction in transversally graded laminates (*TG laminates*) by Jędrysiak and Radzikowska [3, 4, 5] and in longitudinally graded composites by Michalak and M. Woźniak [7], Michalak, Cz. Woźniak and M. Woźniak [8]. Some additional examples of applications of this technique for composites can be found in the books [6, 10].

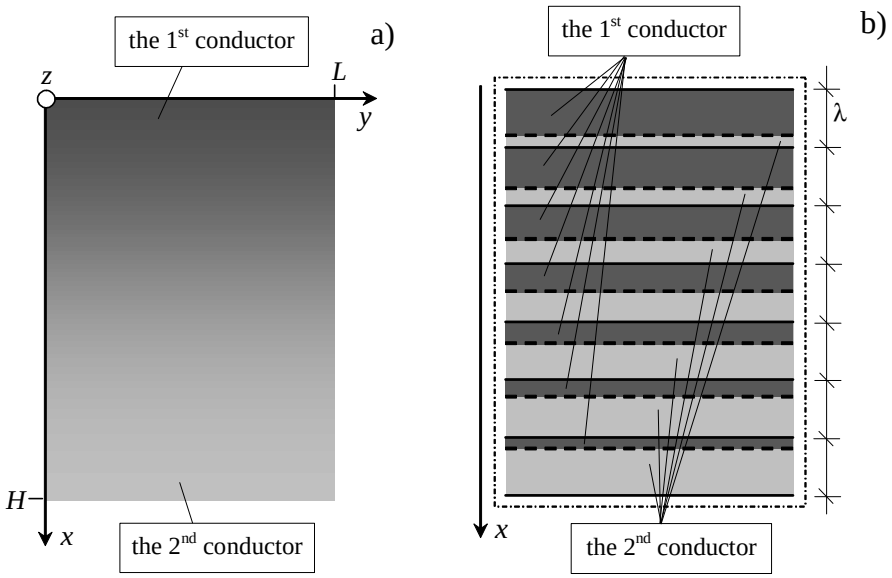

Fig. 1. A cross section of a laminate: a) the macroscopic point of view, b) the microscopic point of view

The main aim of this contribution is to apply the tolerance model equations of heat conduction for laminates with functionally graded properties to analyse stationary heat conduction.

2. TOLERANCE MODELLING

2.1. Modelling foundations

Let subscripts *i*, *j* related to the coordinate system *Oxy*, run over 1, 2. Introduce denotations: ∂_1 as a derivative of *x*; ∂_2 as a derivative of *y*. Let *H* be the laminate thickness along the *x*-axis, and *L* be the length dimension along the *y* axis. We assume that the laminate under consideration occupies the region $\Omega\times\Xi$ on the plane *Oxy*, where $\Omega\equiv(0,H)$, $\Xi\equiv(0,L)$. This laminate is made of two conductors distributed in *m* laminas with the constant thickness λ. Properties of these conductors are described by: specific heats c', c'' and heat conduction tensors with the components k'_{ij}, k''_{ij} $i,j=1,2$. It is assumed that the thickness λ satisfies the condition $\lambda<<H$ and is called *the microstructure parameter*. Every n^{th} lamina consists of two homogeneous sublaminas with thicknesses: λ'_n and $\lambda''_n=\lambda-\lambda'_n$, which are not constant, cf. Fig. 1b. We can introduce the material volume fractions in the n^{th} lamina defined as $\nu'_n\equiv\lambda'_n/\lambda$, $\nu''_n\equiv\lambda''_n/\lambda$. Sequence $\{\nu'_n\}$, $n=1,\ldots m$, is monotone and satisfies the condition $|\nu'_{n+1}-\nu'_n|<<1$, for $n=1,\ldots,m$-1. Because $\nu'_n+\nu''_n=1$ sequence $\{\nu''_n\}$ satisfies similar conditions. Sequences $\{\nu'_n\}$, $\{\nu''_n\}$, $n=1,\ldots m$, can be approximated by continuous functions $\nu'(\cdot)$, $\nu''(\cdot)$, describing the gradation of material properties along the *x* axis. The functions $\nu'(\cdot)$, $\nu''(\cdot)$ can be called *the fraction ratios* of materials. Let us also define the non-homogeneity ratio by $\nu(\cdot)\equiv[\nu'(\cdot)\nu''(\cdot)]^{1/2}$. Moreover, these functions: $\nu'(\cdot)$, $\nu''(\cdot)$, $\nu(\cdot)$, are assumed to be slowly-varying, cf. the book edited by Cz. Woźniak, Michalak and Jędrysiak [10].

Let *T* denote the unknown temperature field. Moreover, the heat conduction problem in the TG laminate will be analysed in the framework of the Fourier's model, i.e. described by the following equation (without heat sources):

$$\partial_i\left(k_{ij}\partial_j T\right)-c\dot{T}=0. \tag{2.1}$$

For the TG laminate all coefficients in equation (2.1), i.e. $k_{ij}=k_{ij}(x)$, $c=c(x)$, are highly-oscillating, tolerance-periodic, non-continuous functions in *x*. Using the tolerance modelling, equation (2.1) can be replaced by the differential equations with continuous, smooth, slowly-varying coefficients, cf. the book edited by Cz. Woźniak, Michalak and Jędrysiak [10] and by Cz. Woźniak et al. [6].

2.2. Concepts and assumptions

The tolerance modelling concepts, the modelling assumptions and the modelling procedure can be found in books [6, 10]. Below, only few of them are reminded.

For an arbitrary integrable function f (which can also depend on y), defined in $\overline{\Omega}$, the averaging operator is given by:

$$< f > (x) = \lambda^{-1} \int_{x-\lambda/2}^{x+\lambda/2} f(\xi) d\xi \tag{2.2}$$

for $x \in [\lambda/2, H-\lambda/2]$. It can be shown that for the tolerance-periodic function f of x, its averaged value calculated from (2.2) is a slowly-varying function in x (cf. the books [6, 10]).

The fundamental modelling assumption is mentioned below.

The assumption is *the micro-macro decomposition*, in the following form:

$$T(x,y) = \vartheta(x,y) + \varphi(x)\psi(x,y), \tag{2.3}$$

where $\vartheta(\cdot,y)$, $\psi(\cdot,y)$ are slowly-varying functions. The basic unknown is function $\vartheta(\cdot,y)$ called *the macrotemperature*; an additional basic unknown is *the fluctuation amplitude* $\psi(\cdot,y)$; $\varphi(\cdot)$ is the known *fluctuation shape function*. The function $\varphi(\cdot)$ is assumed to be continuous, linear across every sublamina thickness and of an order $O(\lambda)$; it can be given by:

$$\varphi(x) = \begin{cases} \lambda\sqrt{3}\,\dfrac{\nu(\bar{x})}{\nu'(\bar{x})}[2x + \nu''(\bar{x})] & \text{for} \quad x \in (-\lambda/2,\, -\lambda/2 + \nu'(\bar{x})) \\ \lambda\sqrt{3}\,\dfrac{\nu(\bar{x})}{\nu''(\bar{x})}[-2x + \nu'(\bar{x})] & \text{for} \quad x \in (\lambda/2 - \nu''(\bar{x}),\, \lambda/2) \end{cases} \tag{2.4}$$

where $\bar{x}$ is a centre of a cell with a length dimension λ and it's independent from x, cf. the book [10].

2.3. Tolerance model equations

Using the tolerance modelling and denoting the smooth functional coefficients: $K \equiv < k_{11} >$, $K_{22} \equiv < k_{22} >$, $\tilde{K} \equiv < k_{11}\partial_1\varphi >$, $\breve{K} \equiv < k_{11}\partial_1\varphi\partial_1\varphi >$, we obtain the averaged heat conduction equations in the form (cf. [3, 4, 5]):

$$\begin{aligned} &\partial_1(K\,\partial_1\vartheta) + K_{22}\,\partial_{22}\vartheta + \partial_1(\tilde{K}\psi) = 0\,, \\ &\tilde{K}\,\partial_1\vartheta + \breve{K}\,\psi - \lambda^2\nu^2 K_{22}\,\partial_{22}\psi = 0\,. \end{aligned} \tag{2.5}$$

Equations (2.5) have the coefficients being slowly-varying functions in x, in contrast to equation (2.1), which has functional, non-continuous, highly oscillating coefficients. Some terms depend explicitly on the microstructure parameter λ.

Equations (2.5) together with the micro-macro decomposition (2.3) constitute *the tolerance model of heat conduction for transversally graded laminates*. These equations take into account the effect of the microstructure size

on heat transfer for these composites. It can be observed that for the TG laminate under consideration boundary conditions for the macrotemperature ϑ have to be formulated on the edges x=0, H and y=0, L, but for the fluctuation amplitude ψ only on the edges y=0, L.

2.4. Applications: stationary heat conduction

Denote by $k'_{11} = k'_{22} = k'$, $k''_{11} = k''_{22} = k''$ heat conduction coefficients in sublaminas and introducing notations:

$K(x) \equiv \nu'(x)k' + \nu''(x)k''$, $\tilde{K}(x) \equiv 2\sqrt{3}\nu(x)(k' - k'')$, $\breve{K}(x) \equiv 12(\nu'(x)k'' + \nu''(x)k')$, equations (2.5) take the form:

$$\begin{aligned} &\partial_1(K\,\partial_1\vartheta) + K\,\partial_{22}\vartheta + \partial_1(\tilde{K}\psi) = 0\,, \\ &\tilde{K}\,\partial_1\vartheta + \breve{K}\,\psi - \lambda^2\nu^2\,K\,\partial_{22}\psi = 0\,. \end{aligned} \tag{2.6}$$

Equations (2.6) together with the boundary conditions were changed to the system of differential equations. A special numerical program based on the finite difference method was written by Mister Artur Wirowski. Using this program, equations (2.6) were solved.

3. RESULTS

In this section some effects of conductor properties c.f. heat conduction coefficients on the laminate temperature are presented.

Let the layer thickness H be coupled with the microstructure parameter λ by the relation $H=m\lambda$ (m is the number of laminas). The fraction ratios of materials are defined as the exponential functions:

$$\nu'(x) = \frac{1-\exp(2x/H)}{1-\exp(2)}, \quad \nu''(x) = 1 - \nu'(x)$$

For the macrotemperature ϑ we assume the following boundary conditions:

a) as a parabolical functions - Fig. 2a and 3a,

$$\vartheta(x,0) = \vartheta(x,L) = 100\left(\frac{x}{H}\right)^2 - 100\frac{x}{H} + 25\,, \quad \vartheta(0,y) = \vartheta(H,y) = 100\left(\frac{y}{L}\right)^2 - 100\frac{y}{L} + 25\,;$$

b) as a constant and a parabolical functions - Fig. 2b and 3b,

$$\vartheta(x,0) = \vartheta(x,L) = 25\,, \quad \vartheta(0,y) = \vartheta(H,y) = 100\left(\frac{y}{L}\right)^2 - 100\frac{y}{L} + 25\,.$$

The boundary conditions are shown as a schema in Fig. 4a,c. For the fluctuation amplitude ψ the boundary conditions we assume as equal zero.

Some calculation results are shown in Fig. 2-3. These plots are made for $L=H$, $m=20$, thus the ratio $\lambda/H=0.05$. In a numerical program the division for H it is 4000, for L – 30. In Fig. 2 there are presented the temperature distributions for the ratio $k''/k'=10$, but Fig. 3 shows plots of the temperature for the ratio $k''/k'=0.1$.

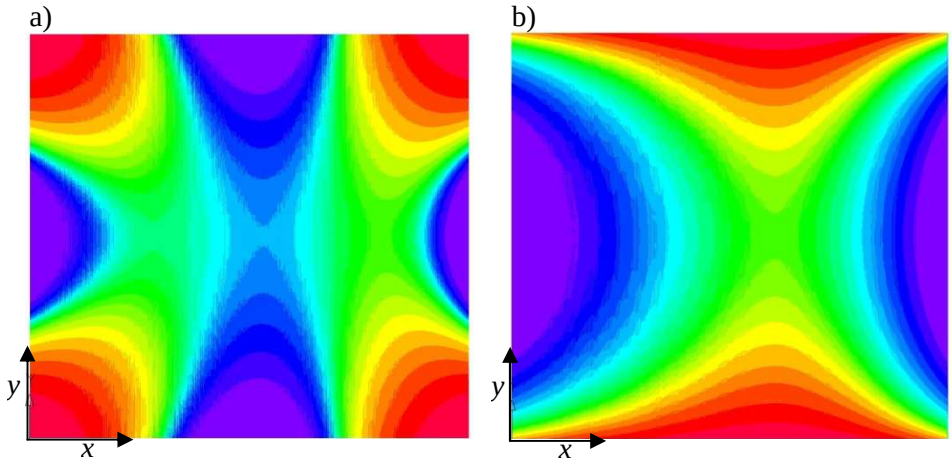

Fig. 2. Temperature distributions for the ratio $k''/k'=10$: a) for boundary conditions shown as a schema in Fig. 4a; b) for boundary conditions shown as a schema in Fig. 4c.

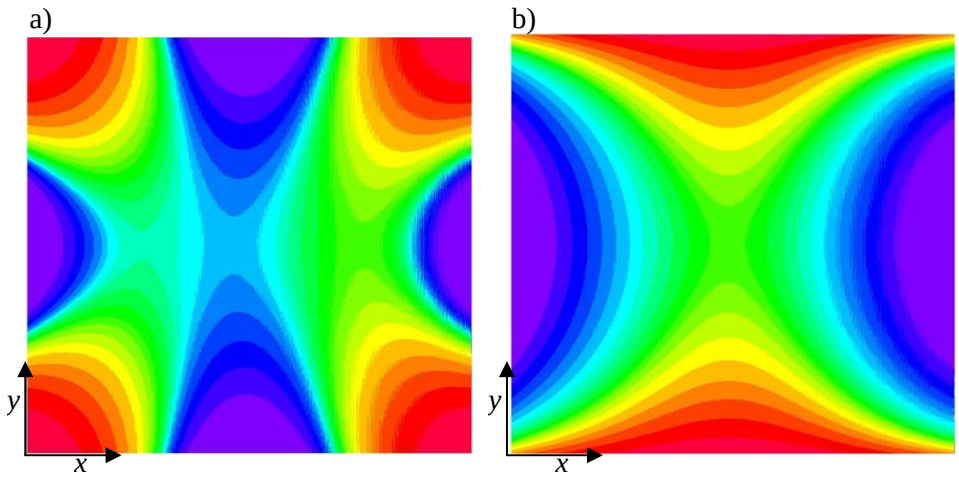

Fig. 3. Temperature distributions for the ratio $k''/k'=0.1$:
a) for boundary conditions shown as a schema in Fig. 4a;
b) for boundary conditions shown as a schema in Fig. 4c.

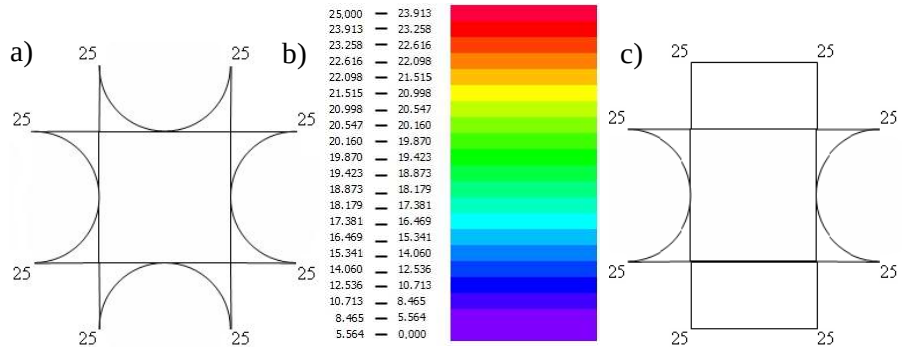

Fig. 4. Schema of the boundary conditions for the macrotemperature ϑ (a), (c) and the legend of the coloring plots (b).

4. REMARKS

Under the calculation results for the stationary heat conduction, we can observe:

- Distributions of the temperature:
  - depend on the differences between heat conduction coefficients k', k'',
  - are symmetric along the y axis,
  - are not symmetric along the x axis, because of the laminas distribution.

The tolerance averaging technique it seems to be an effective tool to research heat conduction in transversally graded laminates.

ACKNOWLEDGEMENTS

The Ministry of Science and Higher Education of Poland support this contribution - grant No. N N506 398535.

The coloring plots are made thanks to the Autodesk Civil 2010 System.

LITERATURA

1. Aboudi J., Pindera M.-J., Arnold S.M.: *Higher-order theory for functionally graded materials*, Composites. Part B, **30** (1999) 777-832.
2. Bansal Y., Pindera M.-J.: *Efficient reformulation of the thermoelastic higher-order theory for functionally graded materials*, J. Therm. Stresses, **26** (2003) 1055-1092.
3. Jędrysiak J., Radzikowska A.: *On the modelling of heat conduction in a non-periodically laminated layer*, J. Theor. Appl. Mech., **45** (2007) 239-257.
4. Jędrysiak J., Radzikowska A.: *Stationary heat conduction in a laminate with functionally graded macrostructure (FGM)*, Build. Phys. Theory Pract., **3** (2008) 23-26.

5. Jędrysiak J., Radzikowska A.: *Some problems of heat conduction for transversally graded laminates with non-uniform distribution of laminas*, Arch. Civil Mech. Engin., (in the course of publication).
6. *Mathematical modelling and analysis in continuum mechanics of microstructured media*, eds. Cz. Woźniak, et al., Publishing House of Silesian University of Technology, Gliwice 2010.
7. Michalak B., Woźniak M.: *On the heat conduction in certain functionally graded composites*, in: Selected Topics in the Mechanics of Inhomogeneous Media, eds. Cz. Woźniak, R. Świtka, M. Kuczma, University of Zielona Góra 2006, 229-238.
8. Michalak B., Woźniak Cz., Woźniak M.: *Modelling and analysis of certain functionally graded heat conductor*, Arch. Appl. Mech., **77** (2007) 823-834.
9. Suresh S., Mortensen A.: *Fundamentals of functionally graded materials*, Cambridge, The University Press 1998.
10. *Thermomechanics of microheterogeneous solids and structures. Tolerance averaging approach*, eds. Cz. Woźniak, B. Michalak, J. Jędrysiak, Wydawnictwo Politechniki Łódzkiej, Łódź 2008.

DWUWYMIAROWE ZAGADNIENIE PRZEWODNICTWA CIEPŁA W LAMINACIE O FUNKCYJNEJ GRADACJI WŁASNOŚCI

S t r e s z c z e n i e

Przedmiotem rozważań pracy jest przewodnictwo ciepła w klasycznym, fourierowskim sformułowaniu, odniesione do laminatu z jednokierunkową funkcyjną gradacją własności. Rozpatrywany jest laminat złożony z wielu dwuskładnikowych warstw, którego właściwości termiczne zmieniają się funkcyjnie w kierunku prostopadłym do laminowania. W pracy zajęto się przypadkiem, gdy grubość warstw jest stała, a każda warstwa złożona jest z dwóch różnych, jednorodnych i izotropowych materiałów. W skali makro własności laminatu zmieniają się w sposób ciągły i gładki wzdłuż kierunku prostopadłego do laminowania. W mikroskali laminat ma budowę określoną przez jednorodne funkcje rozkładu materiałów, dobrane tak, aby sąsiednie warstwy „mało" się od siebie różniły. Celem pracy jest analiza stacjonarnego, dwuwymiarowego zagadnienia przewodnictwa ciepła z użyciem techniki tolerancyjnego uśredniania. Technika ta pozwala zastąpić równanie przewodnictwa ciepła o silnie oscylujących, nieciągłych współczynnikach funkcyjnych układem równań różniczkowych o współczynnikach funkcyjnych gładkich i wolnozmiennych. Otrzymany układ równań rozwiązano metodą różnic skończonych. Przedstawiono rozkłady temperatury w zależności od proporcji między współczynnikami przewodzenia ciepła, przy różnych warunach brzegowych.

CIVIL AND ENVIRONMENTAL ENGINEERING REPORTS

No. 8 2012

THE EFFECT OF THE ADDITION OF CELLULOSE ON THE QUALITY AND THERMAL PROPERTIES OF STRAW BEDDING

Oryna SŁOBODZIAN-KSENICZ
University of Zielona Góra, Faculty of Civil and Environmental Engineering,
Institute of Environmental Engineering
Szafrana st 15, 65-516 Zielona Góra, Poland

The objective of the study was to determine the effect of the addition of recycled cellulose on the quality and temperature of the straw bedding. Starting from week 2 of the production cycle temperatures were registered and the degree of encrustation of both the cellulose and straw bedding was determined. The cellulose bedding was characterized by higher temperatures throughout the production cycle except for weeks 10., 12., 13. and 14. The warmer bedding meant that the appearing encrustation did not restrict the diffusion of vapour and gases. It exhibited more beneficial, aerobic conditions for exothermic processes. The narrower span of temperatures indicates a more uniform temperature of the cellulose bedding. The flock reared on the warmer and better-quality cellulose bedding reached higher final body weight.

Keywords: recycled cellulose, straw, bedding, encrustation, temperature

1. INTRODUCTION

The deep litter systems of managing animals are among the most commonly used in poultry production [2, 11]. The litter is primarily used to ensure the animals proper isolation from the floor as well as moisture absorbency and evaporation [1]. Excessive moisture in the bedding can lead to its lumping and even the forming of thick compact crust on its surface [2, 4, 8]. Cold and low-quality bedding contributes to muscles and feet conditions in poultry (FPD), plumage defects or breast blisters, which lower the carcass class [7, 13].

Therefore, good bedding material should, as long as it is possible, preserve its physical structure conducive to the diffusion of the bedding - air gases as well as provide the animals with warm and comfortable lying area.

The quality and temperature of the bedding is important not only during growing but also during the fattening stage as animals are in direct contact with

it and also because currently bred broilers are less tolerant of unfavourable environmental conditions [8, 9, 12].

Of numerous bedding materials (incl. sand, wood shavings, corncobs, tree bark) [5] straw is the most frequently used one [3, 7]. Since straw is characterized by very average sorptive properties, in order to improve those, a variety of supplements are added to the straw bedding [6, 10]. As confirmed by research, straw beddings with the addition of brown coal and a bacterial vaccine were characterized by higher temperatures, which was beneficial for their quality [11].

The objective of the study was to determine the effect of the addition of recycled cellulose[1] on the quality and temperature of the straw bedding during the growing and fattening of turkey pullets in the long fattening system.

2. MATERIALS AND METHODS

The study was conducted at a livestock facility – a turkey house, consisting of two sectors, 550m² of area each. The first sector was laid with a 10-cm layer of rye straw, the humidity of this layer was 8% (CSB - control straw bedding). The other sector was laid with a 5-cm layer of rye straw strewn with a 5-cm layer of recycled cellulose, and the humidity of this layer was 6,5% (RCB - recycled cellulose bedding). In either type of bedding, in representative places (not in the vicinity of feeders and drinkers or along the sidewalls and endwalls) a set of two probes were installed at the depth of 5 cm to measure the temperature.

The probes were connected to the HOBO recorder. The recorded temperature values of the studied bedding types throughout the production cycle were analysed with the BoxCar Pro 4.6 program.

On so-prepared beddings 6000 one-day-old BIG-6 turkey hens were placed in each sector respectively.

The production cycle lasted 15 weeks and at week 7 the stock's density was reduced.

The feeding, watering, heating and ventilation systems as well as the lighting and feeding programmes in both sectors were the same.

Starting from week 2. of the production cycle, every week, in 6 representative places in either sector, the degree of encrustation was determined according to a 10-point scale, on which each following degree includes the previous ones:

0 - no encrustation,
1 - an approx. 20-cm ring of encrustation around feeders and drinkers,
2 - a 50-cm strip of encrustation along the endwalls,

[1] In this experiment the cellulose was used in the form of a wad, which is safe for the health and welfare of turkeys.

3 - invisible yet foot-detectable crust on 50% of the bedding surface,
4 - invisible yet foot-detectable crust on 80% of the bedding surface,
5 - invisible and thin yet foot-detectable crust on 100% of the bedding surface,
6 - as above but crust readily detectable for feet, ≤ 5cm thick,
7 - visible patches of crust on 50% of the bedding surface (approx. 5cm thick),
8 - visible patches of crust on 100% of the bedding surface (approx. 5cm thick),
9 - 100% of the bedding surface covered with hard compact crust (approx. ≤ 7cm thick),
10 - as above but the crust approx. 10cm thick.

After the production cycle had been finished, samples of the bedding were taken in order to determine its moisture levels. Control measurements of the temperature and air humidity inside the building, in the animal area, were also taken. With the production cycle finished, the birds' body weight was measured by weighing approx. 1900 heads from either sector.

For statistical analysis the STATISTICA 9.1a. program suite was used.

3. RESULTS AND DISCUSSION

Table 1. compares the mean temperature values for the cellulose bedding (RCB) and the straw bedding (CSB) in the analysed weeks of the production cycle.

Week of production cycle	Bedding type	
	RCB	CSB
	Temperature [^{o}C]	
II	29,5	28,6
III	28,6	27,9
IV	25,8	22,6
V	24,3	22,1
VI	23,3	20,5
VII	22,1	20,5
VIII	21,3	20,5
IX	20,5	19,7
X	19,7	20,0
XI	19,9	19,9
XII	20,1	20,1
XIII	20,2	20,6
XIV	20,3	20,7
XV	20,4	20,3

Source: author's calculations

As confirmed by the data in table 1. the cellulose bedding, as compared with the straw bedding, was characterized by higher temperature values throughout the production cycle except for weeks 10., 12., 13. and 14.

At weeks 2. and 3. of the turkeys' growing the temperature of RCB was higher than that of CSB by 0,85 and 0,71^{o}C respectively. The statistical analysis showed that these were not statistically significant differences.

The temperature of RCB at weeks 4. and 5. was higher than that of CSB by 3,2 and 2,15^{o}C respectively. These were statistically highly significant differences ($p<0,001$).

In the subsequent weeks 6. and 7. of the production cycle the temperature of RCB was higher than that of CSB by 2,78 and 1,62^{o}C respectively. These were statistically highly significant differences ($p<0,001$).

At weeks 8. and 9. of the fattening stage the temperature of RCB was also higher than that of CSB by 0,98 and 0,72^{o}C respectively. The statistical analysis showed that these were not statistically significant differences.

At week 10. of the production cycle the temperature of RCB was lower by 0,33^{o}C than that of CSB. This was not a statistically significant difference.

At week 11. of fattening the temperatures of the studied bedding types were similar (difference: 0,03^{o}C). At weeks 12., 13. and 14. of the production cycle RCB was characterized by lower temperature values than CSB, however the differences of 0,06, 0,42 and 0,4^{o}C respectively were not statistically significant. In the last week 15. of the fattening stage the temperature of RCB was higher than that of CSB by 0,3^{o}C. This was not a statistically significant difference.

In the course of the production cycle the temperatures of both bedding types were decreasing - the drop was 9,05^{o}C for RCB and 8,33^{o}C for CSB. The decreasing temperatures of the beddings are partly due to the fall in air temperature in the turkey house (from 34,9^{o}C to 18,2^{o}C in the RCB sector and from 34,8^{o}C to 15,7^{o}C in the CSB sector). A decrease in temperature of the bedding during the production cycle is beneficial as growing animals are becoming less particular about thermal conditions; they can also give up the excess of heat to the colder litter.

Higher temperatures of both bedding types starting with week 12. of fattening despite lower temperature values of the environment indicate that there were exothermic processes taking place in both beddings.

Table 2. compares the minimal and maximum temperature values of the studied bedding types and the temperature spans in the analysed weeks of the production cycle.

Week of production cycle	RCB			CSB		
	Temperature [^{o}C]					
	Min	Max	R	Min	Max	R
II	27,89	30,39	2,5	27,18	30,25	3,07
III	27,21	29,76	2,55	26,49	30,55	4,06
IV	24,34	27,14	2,80	21,46	23,73	2,27
V	22,65	25,82	3,17	21,33	23,15	1,82
VI	22,51	24,45	1,94	16,49	21,84	5,35
VII	21,26	22,67	1,41	18,28	21,70	3,42
VIII	20,40	22,71	2,32	18,28	21,52	3,24
IX	19,45	21,89	2,44	19,04	20,78	1,74
X	19,11	20,71	1,60	19,12	20,68	1,56
XI	18,10	20,75	2,65	18,54	20,87	2,33
XII	19,55	20,30	0,75	19,58	20,46	0,88
XIII	19,58	21,15	1,57	19,89	21,27	1,38
XIV	19,79	21,14	1,35	20,14	21,75	1,61
XV	19,24	21,21	1,97	19,98	21,20	1,22

Source: author's calculations

At weeks 2., 3., 6., 7., 8. and 14. of the production cycle RCB was characterized by a narrower spans of temperatures than CSB. At weeks 10., 12. and 13. temperature spans were similar for both RCB and CSB.

At weeks 4., 5., 9., 11. and 15. of the production cycle the cellulose bedding was characterized by a wider span of temperatures as compared to CSB.

The narrower span of temperatures of the RCB (from 0,75 to 3,17°C) as compared to CSB (from 1,22 to 5,35°C) points to a more uniform temperature of the bedding with the addition of cellulose.

Beddings with even temperatures create more beneficial conditions for a uniform distribution of birds over the whole area of the house, especially in the initial weeks of the cycle.

Table 3. Degree of encrustation of cellulose bedding (RCB) and straw bedding (CSB) in the consecutive weeks of production cycle [10-point scale]

Bedding type	Week of production cycle													
	II	III	IV	V	VI	VII	VIII	IX	X	XI	XII	XIII	XIV	XV
	Degree of encrustation on 10-point scale													
RCB	0	0	0	1	1	2	3	5	5	6	7	9	10	10
CSB	0	1	2	4	4	6	7	8	9	10	10	10	10	10

Source: author's calculations

Table 3. presents the degree of encrustation of the studied bedding types in the analysed weeks of the production cycle. In the cellulose bedding the first signs of encrustation were observed at week 5. of the cycle, whereas in the straw bedding already at week 3. of the growing stage. The process of encrustation advanced consecutively on both bedding types but much more slowly so on the cellulose bedding than on the straw bedding. It was not until week 14. of fattening that the cellulose bedding was covered with thick compact crust (degree 10), whereas on the straw bedding degree 10. of encrustation was found at week 11. of the cycle.

The more slowly advancing encrustation of the cellulose bedding did not restrict the diffusion of vapour and gases between the litter and the air in the building, thus the cellulose bedding exhibited more beneficial, aerobic conditions for exothermic processes. It was confirmed by the lower moisture level in RCB (58,2%) as compared with CSB (59,9%) as well as by the higher temperature levels of RCB than CSB (except for four weeks).

The final body weight of turkey hens reared on the warmer and better-quality cellulose bedding was 10,59 kg and was higher by 0,56 kg as compared to the hens reared on the straw bedding (10,03 kg).

4. SUMMARY AND CONCLUSIONS

The conducted study has shown that in the first seven weeks of the production cycle the cellulose bedding was characterized by higher temperatures than the straw bedding. The statistical analysis showed that the temperature differences between RCB and CSB were highly significant at weeks 4., 5., 6. and 7 ($p<0,001$).

Due to higher temperatures the cellulose bedding was subject to slower encrustation, with degree 1 of encrustation not found until week 5. of the cycle, whereas at the same time in the straw bedding it reached degree 4.

At weeks 8., 9., 11. and 15. of the cycle the temperatures of the cellulose bedding were higher than of the straw bedding, yet the statistical analysis showed that these were not statistically significant differences.

At weeks 10., 12., 13. and 14. of fattening the cellulose bedding was characterized by lower temperature values than the straw bedding. The statistical analysis showed that these were not statistically significant differences.

Despite slightly lower temperatures the cellulose bedding was still subject to slower encrustation than the straw bedding, which at week 11. was covered over its whole area with thick compact crust (degree 10). The last degree 10 of encrustation was not found in the cellulose bedding until week 14. of the fattening stage.

The more slowly advancing process of encrustation in the cellulose bedding than in the straw bedding did not restrict the diffusion of vapour and

gases between the litter and the air in the building, thus the cellulose bedding exhibited more beneficial, aerobic conditions for exothermic processes and water evaporation. With the production cycle finished, the cellulose bedding was less moist than the straw bedding.

The narrower span of temperatures of the cellulose bedding as compared to the straw bedding points to a more uniform temperature of the bedding with the addition of cellulose.

Beddings with even temperatures create more beneficial conditions for a uniform distribution of birds over the whole area of the house.

The flock reared on the warmer and better-quality cellulose bedding reached higher (by 0,56 kg) final body weight than the flock managed on the straw bedding.

REFERENCES

1. Agfact A5.1.9 (Frst edition 1987. Reviewed April 2004): *Alternative litter materials for poultry*. I.S. Embury, Former, Livestock Officer (Poultry) Division of Animal Production.
2. ATAPATTU N.S.B.M., WICKRAMASINGHE K.P.: *The use of refused tea as litter material for broiler chickens* [online]. Poultry Science Association. Vol. 86, No. 5 (2007) 968-972.
3. DOBRZAŃSKI Z., RUDZIK F.: *Jakość ściółki drobiowej – problem wciąż aktualny*. Polskie Drobiarstwo, 5 (1998) 3-6.
4. GRIMES J.L., SMITH J., WILLIAMS C.M.: Some *alternative litter materials used for growing broilers and turkeys.* World's Poultry Science Journal. Vol. 58. no.4 (2002) 515-526.
5. HUANG Y., Yoo J.S., KIM H.J., WANG Y., CHEN Y.J, CHO J.H., KIM I.H.: *Effect of bedding types and different nutrient densities on growth performance, visceral organ weight, and blood characteristics in broiler chickens.* Journal. Applied Poultry. Research Vol. 18. No. 1 (2009) 1-7.
6. *Standardy higieniczne, dobrostan zwierząt oraz ochrona środowiska w produkcji zwierzęcej w świetle przepisów UE.* Red. KOŁACZ R.. F.P.H. ELMA. Wrocław 2000.
7. KUCZYŃSKI T.: *Emisja amoniaku z budynków inwentarskich a środowisko*. Redakcja Wydawnictw Naukowo-Technicznych. Zielona Góra 2002.
8. MALONE B.: *Managing built-up litter*. Proceedings to 2006 Midwest Poultry Federation Conference. 2006.
9. RADOŃ J., BIEDA W., NAWALANY G.: *Broiler house microclimate in light of experimental studies*, Electronic Journal of Polish Agricultural Universities. Vol. 7. Iss. 2 (2004).
10. RITZ C.W., FAIRCHILD B.D., LACY M.P.: *Litter quality and broiler performance* 2005.

11. SŁOBODZIAN-KSENICZ O., KUCZYŃSKI T., HOUSZKA H.: *Evaluating the thermal properties of bedding materials used in poultry production as based on thermovision images,* Problemy Inżynierii Rolniczej Nr 1 (2005) 99-106.
12. SKOMORUCHA I., MUCHACKA R., SOSNÓWKA-CZAJKA E., HERBUT E.: *Response of broiler chickens from three genetic groups to different stocking densities,* Annals of Animal Sciences. Vol. 9. No. 2 (2009) 175–184.
13. YOUSSEF I.M.I., BEINEKE A., ROHN K., KAMPHUES J.,: *Experimental study on effects of litter material and its quality on foot pad dermatitis in growing turkeys*, International Journal of Poultry Science, 9 (2010) 1125-1135.

WPŁYW DODATKU CELULOZY NA JAKOŚĆ I WŁASNOŚCI TERMICZNE PODŁOŻA SŁOMIASTEGO

Streszczenie

Przeprowadzone badania miały na celu określenie wpływu dodatku celulozy pochodzącej z recyklingu, na jakość i własności termiczne podłoża słomiastego. W sektorze RCB indyczki utrzymywano na słomie z celulozą, w sektorze CSP tylko na słomie (sektor kontrolny). Od drugiego tygodnia cyklu produkcyjnego rejestrowano temperatury oraz określano stopień zaskorupienia podłoża celulozowego i słomiastego. Podłoże celulozowe miało wyższe temperatury w całym cyklu produkcyjnym, z wyjątkiem 10., 12., 13. i 14. tygodnia. Na cieplejszym podłożu celulozowym wolniej powstająca skorupa nie ograniczała dyfuzji pary wodnej i gazów. Panowały w nim korzystniejsze, aerobowe warunki dla przemian egzotermicznych. Węższe obszary zmienności temperatur wskazują na bardziej wyrównaną temperaturę podłoża z dodatkiem celulozy. Stado utrzymywane na cieplejszym oraz o lepszej jakości podłożu celulozowym osiągnęło wyższe masy końcowe.

CIVIL AND ENVIRONMENTAL ENGINEERING REPORTS

No. 8 2012

COMPARISON OF THE CALCULATION RESULTS OF HEAT EXCHANGE BETWEEN A SINGLE-FAMILY BUILDING AND THE GROUND OBTAINED WITH THE QUASI-STATIONARY AND 3-D TRANSIENT MODELS. PART 1: CONTINUOUS HEATING MODE

Anna STASZCZUK*
University of Zielona Góra, Faculty of Civil and Environmental Engineering,
Institute of Building Engineering
Szafrana st 1, 65-516 Zielona Góra, Poland

The paper provides comparative results of calculations of heat exchange between ground and typical residential buildings using simplified (quasi-stationary) and more accurate (transient, three-dimensional) methods. Such characteristics as building's geometry, basement hollow and construction of ground touching assemblies were considered including continous heating mode. The calculations with simplified methods were conducted in accordance with currently valid norm: PN-EN ISO 13370:2008. *Thermal performance of buildings. Heat transfer via the ground. Calculation methods.* Comparative estimates concerning transient, 3D, heat flow were performed with computer software WUFI®plus. The differences of heat exchange obtained using more exact and simplified methods have been specified as a result of the analysis.

Keywords: heat transfer via the ground, quasi-stationary calculations, transient heat flow, continous heating mode

1. INTRODUCTION

The heat flow process in the ground is generally transient, three-dimensional and boundary conditions are very complicated.

Recent methods up to the current standard [12] and their derivatives [10], [11] regarding heat exchange between a building and a ground are based on

* Corresponding author. E-mail: A.Staszczuk@ib.uz.zgora.pl

quasi-stationary method developed in the eighties last century by Hagentoft [4], [5], [9] and completed by Anderson [2], [3].

This method assumes harmonic boundary conditions. Annual temperature course including both external and internal temperatures should be in the shape of sinusoid. Indeed, typical mean year pattern of outer air temperature for European location (see Figure 1) can well be approximated by sine curve. If the real conditions, however they are not compatible with this assumption, calculations results may become not accurate and not adequate to simulate heat flow between the building and the ground.

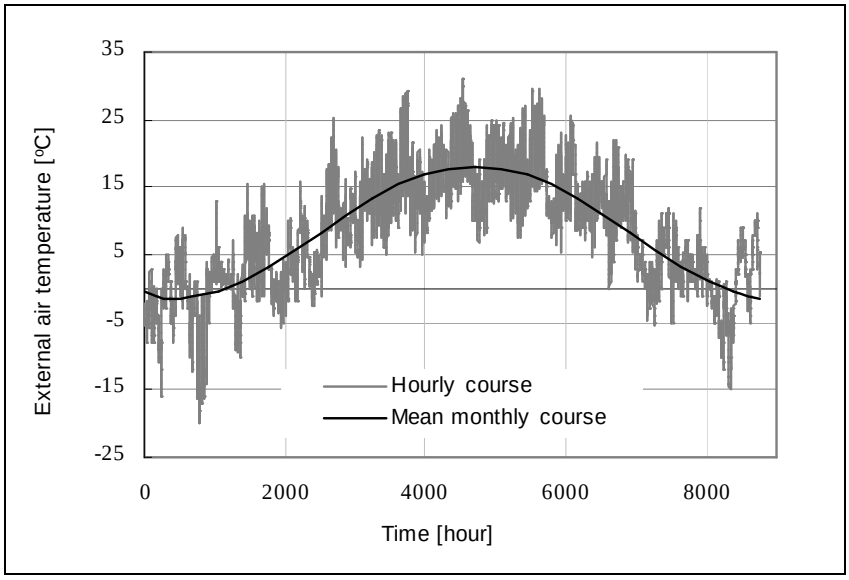

Fig. 1. Yearly pattern of air temperature in Cracow.

In this paper the impact of building's geometry, basement hollow, construction of ground touching assemblies were considered to asses the possible error using quasi-stationary calculation methods for heat exchange with the ground.

Calculations were done for buildings heated continuously according to assumptions in Hagentoft's method (internal air temperature is constant and amplitude of internal air temperature is assumed zero).

The other cases: intermittent heating (cut off 10 p.m – 6 a.m) and reduced heating (with long break e.g. holiday) will be treated (covered) in Part II of this article.

2. MATERIAL AND METHODS

2.1. Calculation tools

Calculations according to PN-EN ISO 13370:2008 [12] were carried out using Microsoft® Excel® software. For calculations of transient, 3D, heat flow through the ground the computer program WUFI®plus was used. The calculations are based on control volume heat balance method [7]. Division of heat conducting space into balance-differential elements with variable grid is done automatically by the program. To obtain realistic predictions of the internal air temperature (especially during intermittent heating), the buildings were calculated with full thermal coupling with the ground. The basement is considered as integral part of the heated building (1 zone model).

The example of modeling of surrounding ground and building for thermal calculation in WUFI®plus software is shown in Figure 2. Thermal coupling is established by defining of internal air temperature as boundary condition for floor and basement walls inside the building. Heat exchange with these assemblies is attributed to zone air node. At certain distance from the building (at least half of a width and at least of a lenght) a vertical adiabatic surface is assumed (no horizontal heat flow). Horizontal adiabatic surface (no vertical heat flow) is assumed at 10m below floor level (at this level ground temperature is assumed to be equal to average external air temperature).

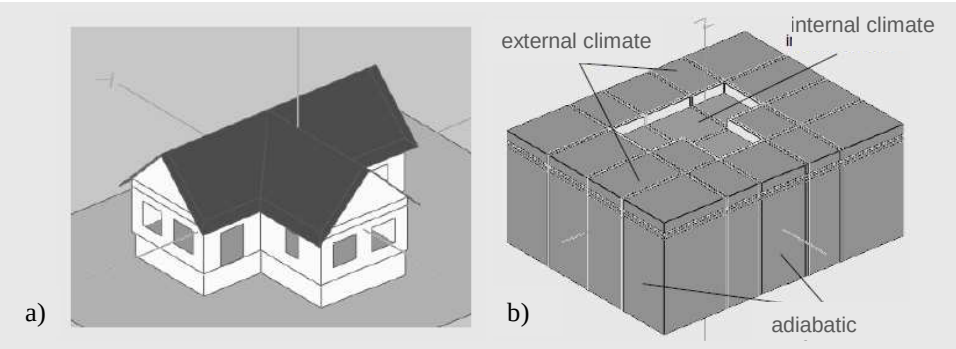

Fig. 2. Modelling of building and ground in WUFI®plus software:
a) building construction, b) 3-D model of surrounding ground.

2.2. Assumptions

The parameters of statistical climate recently developed for Cracow City by Gawin & Kossecka [8] were used as an external boundary condition for the building and ground. The buildings were calculated only thermally according to the WUFI®plus model (www.WUFI.de), using 1 hour time step. Inner air

temperature was obtained iteratively from heat balance of conditioned zone. The heat balance consists of heat exchange with thermal envelope including floor and basement walls, ventilation, solar and internal gains according to EN-ISO 13790 standard [6]. Despite variable spatial division the number of differential ground elements extended from about 100 to 160 thousand. Set point of inner air temperature of 20°C and minimal air exchange rate of 1,0 ACH were assumed.

2.3. Cases

Three types of typical ground-floor residential buildings, characterized by different geometry (see Figure 3) were considered.

Observing tendency in the development of the modern single-family housing in Poland, small buildings about the footprints floor area not exceeding 100 m^2 were chosen for analysis. The shapes (footprints) and main dimensions are shown in Figure 3. Thermal insulation level of outside and inside components follows Polish regulations.

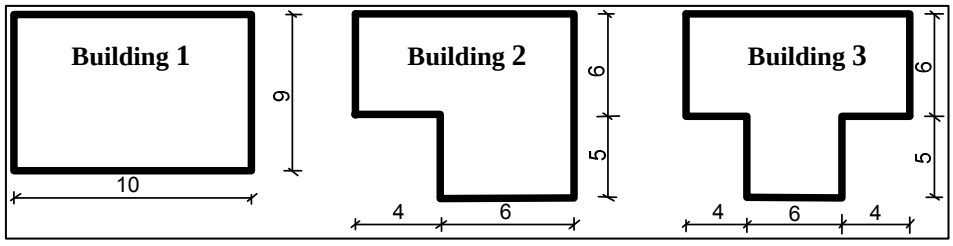

Fig. 3. Shapes of analyzed buildings.

For each building three cases of basement hollow were considered:

- slab on ground (z = 0 m),
- basement (height 2,2 m, z = 1.0 m),
- basement (height 2,2 m, z = 1.5 m),

where “z” means the depth of cellar floor below ground level.

In addition every case includes two scenarios of earth-contact construction:

a - thermally not insulated,

b - thermally insulated (slab on ground insulated with 10 cm EPS, edge vertical insulation 10 cm EPS - 0.7 m depth, floor and basement walls thermally insulated with 5 cm EPS).

3. NUMERICAL ANALYSIS

3.1. Building and ground characteristics

In the Tables 1 and 2 the geometry and assembly construction of exemplary buildings are presented. The same assemblies and material data were assumed in everyone of the presented buildings.

According to PN-EN ISO 13370 standard recommendation thermal conductivity for ground λ=2,0 W/(m·K) and thermal capacity $\rho \cdot c = 2{,}0 \cdot 10^6$ J/(m3·K) were used.

Table 1. Building geometry

Specification	Building 1 Rectangular	Building 2 „L-shaped”	Building 3 „T-shaped”
Floor area [m^2]	74	74	94
Net volume [m^3]:			
- building with floor on ground	252	252	319
- building with basement	447	447	605
Floor perimeter [m]	35	39	47
Characteristic dimension* B’	4,32	3,79	4,03
A/V coefficient:			
- building with floor on ground	1,14	1,18	1,15
- building with basement	0,80	0,84	0,82

**B’ = floor area/(0,5·permieter lenght)*

Table 2. Assemblies and materials

Building component	Material	U [$Wm^{-2}K^{-1}$]
Outer wall	29 cm MAX hollow ceramic bricks + 10 cm EPS	0,29
Floor on ground	Concrete 10 cm	4,30
Foundation	Concrete 29 cm	3,13
Floor on ground thermally insulated	Concrete 10 cm + 10 cm EPS + Concrete 5 cm	0,36
Foundation thermally insulated	Concrete 29 cm + 10 cm EPS	0,35
Basement floor on ground	Concrete 10 cm	4,30
Basement floor on ground thermally insulated	Concrete 10 cm + 5 cm EPS + Concrete 5 cm	0,66

Table 2. Assemblies and materials

Building component	Material	U [$Wm^{-2} K^{-1}$]
Basement wall	Concrete bricks 24 cm	2,19
Basement wall thermally insulated	Concrete bricks 24 cm + 5 cm EPS	0,57
Ceiling up to unheated attic	OSB plate + 18 cm mineral wool + plywood 2 cm	0,20
Ceiling inside balanced zone	Reinforced concrete 15 cm + 5 cm EPS + 5 cm concrete + 2 cm hard wood (parquet floor)	0,55
Windows	Double glazing SHGC (average) = 0.53	1,99

3.2. Calculations

Transient heat flow calculations were made for 2 years period. First year of simulation was used only to define proper initial condition (temperature distribution) in the ground and was not taken into account.

Hourly pattern of both internal and external air temperature obtained with WUFI®plus (transient 3D) calculations was used to define mean year value and amplitude (sine curve for PN-EN ISO 13370 calculation) for every building type and case.

Due to summer overheating inner air temperature has no zero amplitude, even by constant heating throughout a year. Sometimes, however, inner air fluctuations are disregarded when calculating according to the PN-EN ISO 13370 standard. Therefore two kinds of comparative calculation were made, with and without considering the variation of monthly mean internal temperature.

4. RESULTS

To assess influence of the chosen factors on the calculations accuracy of heat exchange between building and the ground, transient heat flow Φ [kW] obtained with WUFI®plus (transient 3D method) was monthly averaged and compared with the results obtained according to the PN-EN ISO 13370 standard (quasi-stationary method).

As a results of analysis, heat exchange between building and the ground Q [kWh] for particular month and for the whole heating season were presented. Percentage value of difference between presented methods was calculated as:

$$\Delta Q_{1-3} = \frac{Q_1 - Q_3}{Q_3}$$

and

$$\Delta Q_{2-3} = \frac{Q_2 - Q_3}{Q_3}$$

where:

Q_1 – heat exchange according to quasi-stationary method without variation of monthly mean internal air temperature, internal air temperature assumed constant [kWh],

Q_2 – heat exchange according to quasi-stationary method with variation of monthly mean internal temperature adopted from WUFI®plus calculations [kWh],

Q_3 – heat exchange according to transient 3D method [kWh],

ΔQ_{1-3} – relative between quasi-stationary (Q_1) and transient 3D (Q_3) methods [%],

ΔQ_{1-2} – relative between quasi-stationary (Q_2) and transient 3D (Q_3) methods [%],

taking that into account transient 3D method is more accurate.

Additionaly, statistical parameters such as: standard deviation (*s*) and correlation coefficient (*r*) were calculated regarding 7 months of heating season. Graphical interpretation of obtained results in statistical approach was presented in box-plots.

As expected, adjustment of the internal temperature provided better results, i.e. ΔQ_{2-3} deviations are generally smaller then ΔQ_{1-3}. However differences between ΔQ_{1-3} and ΔQ_{2-3} are almost negligible. It means that in case of continuous heating internal temperature can be set constant with no effect on the heat loss to the ground. Therefore, in this paper, only differences ΔQ_{1-3} were presented and indicated later on as ΔQ.

In Table 3 calculation results of heat exchange between a building and the ground in heating season for the all considered buildings and cases were presented including both quasi-stationary and transient 3D method.

The most comparable results can be noticed in the case of insulated slab on ground and both not insulated and insulated basement (differences are not greater than ±10%) in the all considered types of buildings. However, heat losses through not insulated slab on ground calculated with simplified method varies from 20% in the case of Building 1 (Rectangular) and Building 2 (L-shaped) to 30 % in the case of Building 3 (T-shaped).

Table 3. Calculation results of heat exchange (Q_1 and Q_3) between the building and the ground in the heating season in Cracow.

Scenario	**Heat exchange between building and the ground**		**Differences in calculations of heat exchange between building and the ground**			
	Quasi-stationary method	Transient 3D method				
	Q_1	Q_3	ΔQ			
	kWh		kWh	**%**	s	r
BUILDING 1						
Slab on the ground						
a	4231,00	3552,11	678,89	19,11	58,15	0,996
b	1086,75	1065,67	21,07	1,98	32,19	0,991
Basement z = 1,0 m						
a	6782,06	6487,09	294,98	4,55	69,62	0,967
b	3220,79	3255,96	-35,17	-1,08	14,98	0,995
Basement z = 1,5 m						
a	7152,45	7243,33	-90,88	-1,25	66,58	0,968
b	3499,10	3688,19	-189,09	-5,13	13,74	0,993
BUILDING 2						
Slab on the ground						
a	4517,71	3651,92	865,79	23,71	72,65	0,995
b	1091,93	1073,28	18,65	1,74	38,02	0,990
Basement z = 1,0 m						
a	7367,71	6924,71	443,00	6,40	85,21	0,986
b	3430,73	3450,50	-19,77	-0,57	20,56	0,994
Basement z = 1,5 m						
a	7783,58	7749,23	34,35	0,44	82,59	0,964
b	3744,50	3924,81	-180,31	-4,59	18,89	0,992
BUILDING 3						
Slab on the ground						
a	5563,29	4354,25	1209,04	27,77	90,45	0,993
b	1383,27	1335,67	47,60	3,56	46,29	0,988
Basement z = 1,0 m						
a	9000,10	8136,18	863,91	10,06	106,77	0,965
b	4228,85	4096,62	132,22	3,2	23,99	0,994
Basement z = 1,5 m						
a	9500,31	9193,78	306,53	3,33	105,07	0,962
b	4605,57	4692,01	-86,44	-1,8	21,96	0,992

Statistical analysis confirms above considerations (see Figure 4). Distribution of differences between analyzed methods (quasi-stationary and transient) is approximately zero in the case of insulated assemblies touching ground.

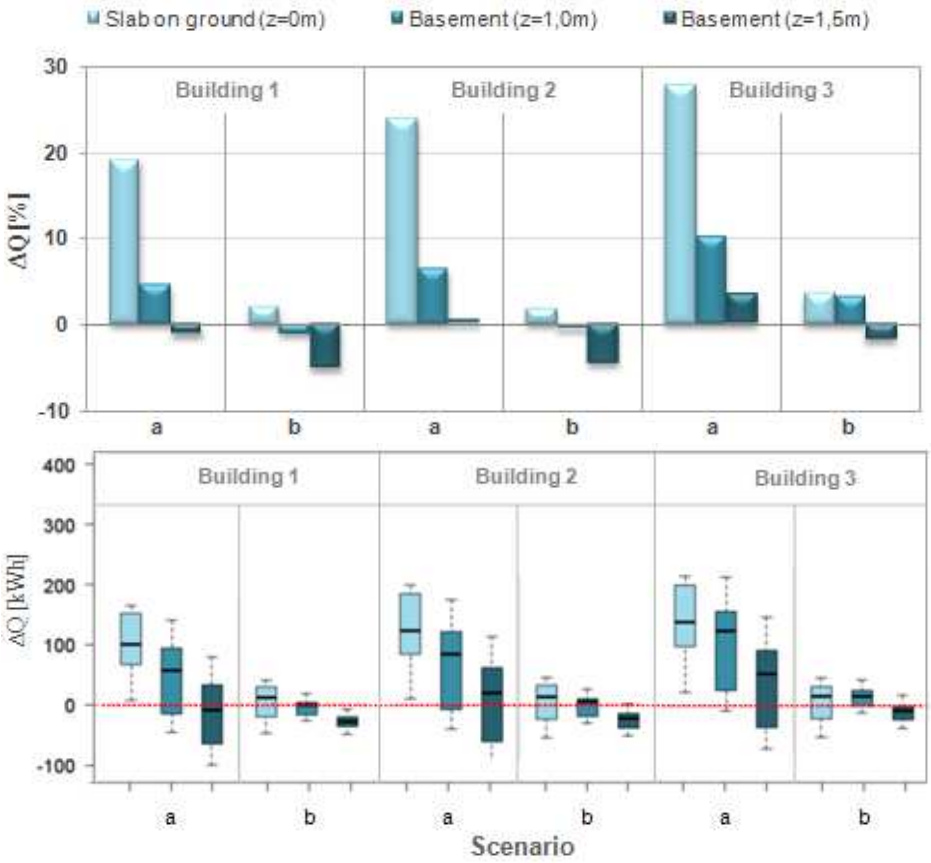

Fig. 4. Differences in heat exchange calculations ΔQ [%] in heating season and their statistical interpretation (*box-plots*).

5. CONCLUSIONS

All considered in the paper factors such as building's geometry, basement hollow and construction of ground touching assemblies have some (less or more) influence on calculation accuracy of quasi-stationary method according to Hagentoft assumptions including continous heating mode.

The highest differences (up to 30%) independent of building type occur in the case of uninsulated slab on ground. However, comparative analysis of different calculation methods carried out by Adjali et all [1] have shown, that calculations according to simplified methods can bring under- or overestimation on such level.

Thermal insulation of assemblies touching ground and building hollow caused incresase of the quasi-stationary calculation accuracy. It is to be

supposed that thermal insulation of slab on ground, foundations, basement floor and walls, and building hollow decrease influence of boundary conditions on heat exchange between building and the ground. Especially significant in the case of slab on the ground. Furthermore, thermal insulation doesn't only reduce both 2-D heat flow at the floor perimeter and 3-D heat flow in the corners, but according to quasi-stationary method it additionally decreases the impact of building's geometry on calculation accuracy. The differences between rectangular L-shaped and T-shaped building are small in comparison with the general accuracy.

Taking into account the above mentioned, as well as more and more restrictive requirements concerning thermal protection of buildings, the analysis of uninsulated assemblies seems to be useless. It also concerns assemblies touching ground. However, the results of research [13] carried out by the author of this paper have shown, that complete or partial resign from ground thermal insulation, directly utilizing ground heat storage capacity, seems to be the most promising solution for decreasing internal air temperature in one-storey residential buildings during the long periods of very high summer temperatures in moderate climate regions.

Generally, differences between analyzed methods considered not exceed ±10% and quasi-stationary calculations according to PN-EN ISO 13370 standard (Hagentoft assumptions) may be useful in enginerring practice.

Appropriate method and calculation tools for assessment of heat loss to the ground come into prominence in energy-saving and proecological building design according to sustainable development paradigm.

REFERENCES

1. Adjali M.H., Davies M, Rees S.W.: *A comparative study of design calculations and measured heat loss through the ground*. Building and Environment, 39 (2004) 1301-1311.
2. Anderson B.R.: *Calculation of the steady-state heat transfer through a slab-on ground floor*. Building and Environment, 26, 4 (1991) 405-415.
3. Anderson B.R.: *The effect of edge insulation on the steady-state heat transfer through a slab-on-ground floor*. Building and Environment, 28, 3 (1993) 361-367.
4. Claesson J.,Hagentoft C-E.: *Heat Loss to the Ground From a Building - I. General Theory*. Building and Environment, 26, 2 (1991) 195–208.
5. Claesson J., Hagentoft C-E.: *Heat Loss to the Ground from a Building - II. Slab on the Ground*. Building and Environment, 26, 4 (1991) 395–403.

6. EN-ISO 13790:2007. *Energy performance of buildings. Calculation of energy use for space heating and cooling.*
7. Gdula S.: *Heat transfer (in polish)*. PWN, Warszawa 1984.
8. Gawin D., Kossecka E.: *Computer building physics. Typical meteorological year for simulation of heat and mass exchange with buildings (in polish).* Drukarnia Wydawnictw Naukowych, Łódź 2002.
9. Hagentoft C-E.: *Heat loss to the ground from a building. Slab on the ground and cellar*. Dissertation, Department of Building Technology, University of Lund 1988.
10. PN-B-02025:2001. *Obliczenia sezonowego zapotrzebowania na ciepło do ogrzewania budynków mieszkalnych i użyteczności publicznej*.
11. PN-EN ISO 12831: 2006. *Instalacje grzewcze w budynkach – Metoda obliczania projektowego obciążenia cieplnego.*
12. PN-EN ISO 13370:2008 *Thermal performance of buildings. Heat transfer via the ground. Calculation methods.*
13. Staszczuk A., Kuczyński T. *The effect of high summer temperatures on slab thermal design in one-storey residential buildings in Poland (in polish).* Izolacje: Budownictwo, Przemysł, Ekologia, 6(2012), s.38-42.

PORÓWNANIE WYNIKÓW OBLICZEŃ WYMIANY CIEPŁA JEDNORODZINNEGO BUDYNKU MIESZKALNEGO Z GRUNTEM UZYSKANYCH ZA POMOCĄ METODY QUASI-STACJONARNEJ ORAZ MODELU NIESTACJONARNEGO TRÓJWYMIAROWEGO. CZĘŚĆ I: OGRZEWANIE CIĄGŁE

S t r e s z c z e n i e

W artykule przedstawiono porównanie wyników obliczeń wymiany ciepła typowego budynku mieszkalnego z gruntem z zastosowaniem metody quasi-stacjonarnej i metody uwzględniającej w pełni niestacjonarny, trójwymiarowy przepływ ciepła w gruncie. Celem analizy obliczeniowej było określenie wpływu wybranych czynników takich jak: geometria budynku, poziom zagłębienia budynku w gruncie oraz konstrukcja przegród stykających się z gruntem na dokładność obliczeń wymiany ciepła za pomocą metod quasi-stacjonarnych uwzględniając ciągły tryb ogrzewania budynku. Obliczenia z zastosowaniem metody uproszczonej przeprowadzono zgodnie z aktualnie obowiązującą normą: PN-EN ISO 13370:2008. W celu przeprowadzenia szczegółowych obliczeń numerycznych opracowano model wymiany ciepła budynku z termicznym sprzężeniem z gruntem, oparty na metodzie bilansów elementarnych i stanowiący integralną część programu komputerowego "WUFI®plus". Rezultatem analizy porównawczej są różnice w wymianie ciepła określonej z zastosowaniem obu metod obliczeniowych.

CONTENTS

❖ CIVIL AND ENVIRONMENTAL ENGINEERING REPORTS ❖